

Physical parameter space of bimetric theory and SN1a constraints

Marvin Lüben,^a Angnis Schmidt-May,^a Jochen Weller^{b,c,d}

^aMax-Planck-Institut für Physik (Werner-Heisenberg-Institut),
Föhringer Ring 6, 80805 Munich, Germany

^bUniversitäts-Sternwarte, Ludwig-Maximilians-Universität München
Scheinerstr. 1, 81679 Munich, Germany

^cExcellence Cluster Origins, Boltzmannstr. 2, D-85748 Garching, Germany

^dMax Planck Institute for Extraterrestrial Physics,
Giessenbachstr. 1, 85748 Garching, Germany

E-mail: mlueben@mpp.mpg.de, angnissm@mpp.mpg.de, jochen.weller@usm.lmu.de

Abstract. Bimetric theory describes a massless and a massive spin-2 field with fully non-linear (self-)interactions. It has a rich phenomenology and has been successfully tested with several data sets. However, the observational constraints have not been combined in a consistent framework, yet. We propose a parametrization of bimetric solutions in terms of the effective cosmological constant Λ and the mass m_{FP} of the spin-2 field as well as its coupling strength to ordinary matter $\bar{\alpha}$. This simplifies choosing priors in statistical analysis and allows to directly constrain these parameters with observational data not only from local systems but also from cosmology. By identifying the physical vacuum of bimetric theory these parameters are uniquely determined. We work out the new parametrization for various submodels and present the implied consistency constraints on the physical parameter space. As an application we derive observational constraints from SN1a on the physical parameters. We find that a large portion of the physical parameter space is in perfect agreement with current supernova data including self-accelerating models with a heavy spin-2 field.

Keywords: Bimetric theory, supernova constraints, cosmology, physical parametrization

Contents

1	Introduction	1
2	Bimetric theory in a brief	2
2.1	Action and equations of motion	2
2.2	Proportional backgrounds and mass spectrum	4
3	Background cosmology	5
3.1	Flat FLRW Ansatz	5
3.2	Equations of motion	5
3.3	Finite and infinite branch	6
4	Unique vacuum and physical parametrization of solutions	7
4.1	Rescaling invariance and natural parameter values	7
4.2	Definition of physical parameters	8
4.3	Consistent vacuum	9
4.4	GR- and massive gravity limit in physical parametrization	10
5	Model-specific considerations	10
5.1	1-parameter model: β_1 -model	11
5.2	2-parameter models	12
5.3	3-parameter models	15
6	Constraints from SN1a	18
6.1	Supernovae Type 1a	18
6.2	Data analysis	18
6.3	Results and discussion	21
7	Conclusions and outlook	24
A	Example: Tuning of the interaction parameters	26
B	Dictionary for the three parameter models	27
C	Details of the scan	30

1 Introduction

The Standard Model of particle physics contains particles with different spin numbers up to 1. For each spin number there are consistent (field) theories describing massless and massive particles. Going higher in the spin number, the theory of General Relativity contains a spin-2 field that is massless, the (yet unobserved) graviton. The question arises whether one can construct a consistent theory describing a spin-2 field that is massive. The first attempt was undertaken by Fierz and Pauli in 1939 who proposed a linear theory [1, 2]. Boulware and Deser argued that any non-linear completion of the linearized theory must contain a ghost [3–6]. However, in 2010/11 a ghost-free and fully non-linear theory describing a massive spin-2 field in flat spacetime was presented usually referred to as (dRGT) massive gravity [7–10]. Hassan and Rosen generalized the theory to bimetric theory that describes a gravitating massive spin-2 field [11, 12]. Massive gravity and bimetric theory hence fill the gap in the list of consistent field theories describing massless and massive particles with spin up to 2. For a review on bimetric theory we refer to Ref. [13].

The massive spin-2 field has various phenomenological implications, from local to cosmological scales. Bimetric theory has cosmological solutions which give rise to an accelerated expansion of the

universe at late times even in the absence of vacuum energy [14–17]. This feature is usually referred to as self-acceleration. Within bimetric theory the interaction energy between the spin-2 fields is responsible for the late time acceleration, besides a possible vacuum energy component. Moreover, bimetric theory contains a Dark Matter candidate, the massive spin-2 field [18–20]. On galaxy cluster to galactic scales, the fifth force mediated by the massive spin-2 field gives rise to beneficial deviations from General Relativity, affecting the required Dark Matter abundance in these systems [21]. On smaller scales the fifth force is suppressed due the Vainshtein screening mechanism [5, 22] as demanded by local tests of gravity [23]. This, however, depends on the mass of the spin-2 field and its coupling strength to ordinary matter. A collection of various phenomenological features of bimetric theory can be found, e.g., in Ref. [24].

In this paper we aim at constraining the physical parameter space of bimetric theory with cosmological data. By physical parameters we mean, e.g., the mass of the massive spin-2 field, m_{FP} , and its coupling strength to matter, $\bar{\alpha}$. Of course, bimetric theory has been compared to cosmological data previously on both the background and perturbative level, see ,e.g., Refs. [14–17, 25–28]. All these studies found various (sub-)models that give rise to a viable background cosmology which can compete with General Relativity. However, the existing results cannot be combined in a straightforward manner due to different parameterizations and assumptions.

To translate the observational constraints coming from cosmology to the physical parameters, these must be related to the parameters of the theory in a unique way. This requires to identify the physical vacuum out of the up to four vacuum solutions of bimetric theory. We do this by imposing theoretical consistency requirements on the vacuum and on the cosmic expansion history. Further we demand that the consistent vacuum corresponds to the infinite future of the viable expansion history which identifies the physical vacuum of bimetric theory. The first aim of this paper is to identify the physical vacuum for all bimetric models with up to three non-vanishing interaction parameters and work out the dictionary between the different parameterizations. Thereby we find theoretical consistency constraints on the physical parameter space. The second aim is to apply this procedure to constrain the physical parameters of these (sub-)models with data from supernovae of Type Ia.

The paper is organized as follows. In section 2 we give a brief introduction to bimetric theory and in section 3 we review FLRW solutions. In section 4 we propose the physical parametrization and explain how to construct it. While in section 5 we apply the procedure to various (sub-)models of bimetric theory, we perform the data analysis for each (sub-)model in section 6. Finally, in section 7 we summarize our results and discuss possible next steps.

2 Bimetric theory in a brief

In this section, we summarize those aspects of bimetric theory needed to study cosmological solutions. After presenting the action and the equations of motion, we discuss vacuum solutions and the mass spectrum of the linearized theory.

2.1 Action and equations of motion

We focus on a version of bimetric theory (so-called singly-coupled) where matter fields couple minimally to only one of the metric tensors¹, say $g_{\mu\nu}$. The ghost-free action is given by [7–11, 40]

$$S = m_g^2 \int d^4x \left[\sqrt{-g} R(g) + \alpha^2 \sqrt{-f} R(f) - 2\sqrt{-g} V(g, f) \right] + \int d^4x \sqrt{-g} \mathcal{L}_m(g, \phi_i) \quad (2.1)$$

¹To which metric the matter fields should couple led to a lot of discussion in the literature [29–34]. The result is that there are only two options which do not reintroduce the Boulware-Deser ghost at unacceptable low energy scales. A matter field can minimally couple to only one of the metric tensors. That allows for two independent matter sectors (one for $g_{\mu\nu}$ and one for $f_{\mu\nu}$) that do not couple directly to each other, but only via their gravitational interactions [29, 30]. The singly-coupled version in which we work in this article is a special case without a $f_{\mu\nu}$ -matter sector. Alternatively, matter can minimally couple to an effective metric composed out of the two metric tensors [29]. This matter coupling lowers the cutoff of the theory but can be embedded into a trimetric setup [31]. Phenomenological aspects were discussed in e.g. Refs. [17, 35–39].

where $R(g)$ and $R(f)$ are the Ricci scalars of the two metric tensors $g_{\mu\nu}$ and $f_{\mu\nu}$, resp. The parameter m_g is the Planck mass of $g_{\mu\nu}$ and the quantity α measures the ratio of m_g to the $f_{\mu\nu}$ -Planck mass. The metric tensors interact via the bimetric potential

$$V(g, f; \beta_n) = \sum_{n=0}^4 \beta_n e_n(S), \quad (2.2)$$

which is defined in terms of the elementary symmetric polynomials e_n [9]. These are functions of the square-root matrix S defined as

$$S^\mu_\alpha S^\alpha_\nu = g^{\mu\alpha} f_{\alpha\nu} \quad (2.3)$$

or in matrix notation, $S = \sqrt{g^{-1}f}$. Due to the properties of the elementary symmetric polynomials, the bimetric potential satisfies the relation

$$\sqrt{-g} V(g, f; \beta_n) = \sqrt{-f} V(f, g; \beta_{4-n}). \quad (2.4)$$

The interaction parameters β_n are constant parameters of mass dimension 2 (in our normalization), where β_0 parametrizes the vacuum energy for $g_{\mu\nu}$ and similarly β_4 for $f_{\mu\nu}$. Matter fields, which we collectively denote as ϕ_i couple minimally to $g_{\mu\nu}$ and \mathcal{L}_m is some generic matter Lagrangian. Therefore, $g_{\mu\nu}$ is the physical metric which defines the geometry in which the matter fields ϕ_i live.

When varying the action (2.1) w.r.t $g^{\mu\nu}$ and $f^{\mu\nu}$, we arrive at two sets of Einstein field equations:

$$G_{\mu\nu} + V_{\mu\nu} = \frac{1}{m_g^2} T_{\mu\nu}, \quad \tilde{G}_{\mu\nu} + \frac{1}{\alpha^2} \tilde{V}_{\mu\nu} = 0 \quad (2.5)$$

where $G_{\mu\nu}$ and $\tilde{G}_{\mu\nu}$ are the usual Einstein tensors of $g_{\mu\nu}$ and $f_{\mu\nu}$, resp. The stress-energy tensor of matter is given by

$$T_{\mu\nu} = -\frac{2}{\sqrt{-g}} \frac{\delta \sqrt{-g} \mathcal{L}_m}{\delta g^{\mu\nu}}. \quad (2.6)$$

The contributions from the bimetric potential are given by

$$V_{\mu\nu} = \sum_{n=0}^3 (-1)^n \beta_n g_{\mu\lambda} Y_{(n)\nu}^\lambda(S), \quad \tilde{V}_{\mu\nu} = \sum_{n=0}^3 (-1)^n \beta_{4-n} f_{\mu\lambda} Y_{(n)\nu}^\lambda(S^{-1}) \quad (2.7)$$

where the explicit form of the function $Y_{(n)\nu}^\lambda$ can be found in, e.g., Ref. [9].

Both Einstein tensors satisfy the Bianchi identities, $\nabla^\mu G_{\mu\nu} = 0$ and $\tilde{\nabla}^\mu \tilde{G}_{\mu\nu} = 0$, where ∇^μ is the covariant derivative compatible with $g_{\mu\nu}$ and $\tilde{\nabla}^\mu$ is the covariant derivative compatible with $f_{\mu\nu}$. If the matter action is invariant under diffeomorphisms, its stress-energy tensor satisfies the conservation equation

$$\nabla^\mu T_{\mu\nu} = 0. \quad (2.8)$$

This results in the *Bianchi constraint* in bimetric theory,

$$\nabla^\mu V_{\mu\nu} = 0, \quad \tilde{\nabla}^\mu \tilde{V}_{\mu\nu} = 0, \quad (2.9)$$

where it can be shown that one equation implies the other due to diffeomorphism invariance.

At this stage, we already note that the action (2.1) is invariant under the map,

$$\sqrt{g^{-1}f} \longrightarrow -\sqrt{g^{-1}f}, \quad \beta_n \longrightarrow (-1)^n \beta_n. \quad (2.10)$$

Suppose, $S = \sqrt{g^{-1}f}$ is a solution to the bimetric field equations with interaction parameters β_n . This solution is dual to the solution $-S$ with interaction parameters $(-1)^n \beta_n$. Hence, considering only half of the solutions already covers the entire solution space for arbitrary interaction parameters. We will come back to this point when studying cosmological solutions. Note that for $\beta_1 = \beta_3 = 0$, eq. (2.10) is a symmetry of the theory.

2.2 Proportional backgrounds and mass spectrum

After having presented the bimetric field equations, let us study an important class of solutions: the proportional background. Let both metrics be related by a conformal factor c as

$$\bar{f}_{\mu\nu} = c^2 \bar{g}_{\mu\nu}. \quad (2.11)$$

The Bianchi constraint forces c to be a constant. The field equations reduce to two sets of Einstein equations,

$$G_{\mu\nu}(\bar{g}_{\mu\nu}) + \Lambda_g \bar{g}_{\mu\nu} = 0, \quad \tilde{G}_{\mu\nu}(\bar{f}_{\mu\nu}) + c^{-2} \Lambda_f \bar{f}_{\mu\nu} = 0. \quad (2.12)$$

The cosmological constants Λ_g and Λ_f originate from the bimetric potential and are given by

$$\Lambda_g = \beta_0 + 3\beta_1 c + 3\beta_2 c^2 + \beta_3 c^3 \quad (2.13a)$$

$$\Lambda_f = \frac{1}{\alpha^2 c^2} (\beta_1 c + 3\beta_2 c^2 + 3\beta_3 c^3 + \beta_4 c^4). \quad (2.13b)$$

Since $G_{\mu\nu}(\bar{g}_{\mu\nu}) = \tilde{G}_{\mu\nu}(\bar{f}_{\mu\nu})$, combining the Einstein equations results in $\Lambda_g = \Lambda_f \equiv \Lambda$, which explicitly reads,

$$\alpha^2 \beta_3 c^4 + (3\alpha^2 \beta_2 - \beta_4) c^3 + 3(\alpha^2 \beta_1 - \beta_3) c^2 + (\alpha^2 \beta_0 - 3\beta_2) c - \beta_1 = 0. \quad (2.14)$$

This is a polynomial in c and has up to four real-valued roots, which determine c in terms of the bimetric parameters, $c = c(\alpha, \beta_n)$. The proportional backgrounds exist only in vacuum; matter stress-energy drives the solution away from the proportional background. Hence, each root c corresponds to a vacuum of bimetric theory. We will study these vacua in more detail in section 4.

Depending on the sign of the effective cosmological constant Λ , the proportional background can describe (Anti-)de Sitter or Minkowski space. Only in such spacetimes a well-defined notion of spin and mass exists due to the presence of Poincare invariance. To find the mass spectrum, we study linear fluctuations around the proportional background,

$$g_{\mu\nu} = \bar{g}_{\mu\nu} + \frac{1}{m_g} \delta g_{\mu\nu}, \quad f_{\mu\nu} = c^2 \bar{g}_{\mu\nu} + \frac{c}{m_f} \delta f_{\mu\nu}, \quad (2.15)$$

where $\delta g_{\mu\nu}$ and $\delta f_{\mu\nu}$ are the canonically normalized linear fluctuations. The mass eigenstates are given by a linear combination of the metric fluctuations [41]

$$\delta G_{\mu\nu} = \frac{1}{\sqrt{1 + \alpha^2 c^2}} (\delta g_{\mu\nu} + \alpha c \delta f_{\mu\nu}), \quad \delta M_{\mu\nu} = \frac{1}{\sqrt{1 + \alpha^2 c^2}} (\delta f_{\mu\nu} - \alpha c \delta g_{\mu\nu}), \quad (2.16)$$

where the mode $\delta G_{\mu\nu}$ describes a massless spin 2-field and the mode $\delta M_{\mu\nu}$ a massive spin 2-field. Its mass in terms of the bimetric parameters is given by

$$m_{\text{FP}}^2 = \left(1 + \frac{1}{\alpha^2 c^2}\right) (\beta_1 c + 2\beta_2 c^2 + \beta_3 c^3). \quad (2.17)$$

The metric fluctuations are a linear superposition of the mass eigenstates,

$$\delta g_{\mu\nu} = \frac{1}{\sqrt{1 + \alpha^2 c^2}} (\delta G_{\mu\nu} - \alpha c \delta M_{\mu\nu}), \quad \delta f_{\mu\nu} = \frac{1}{\sqrt{1 + \alpha^2 c^2}} (\delta M_{\mu\nu} + \alpha c \delta G_{\mu\nu}). \quad (2.18)$$

This allows for a physical interpretation of the combination αc . It measures the mixing of the mass eigenstates in the original metric fluctuations and can be thought of as being related to a mixing angle. In the limit $\alpha c \rightarrow 0$, the massive mode drops out of the fluctuations of the physical metric $g_{\mu\nu}$. Since in singly-coupled bimetric theory matter couples to $g_{\mu\nu}$, we expect to recover the laws of GR in that limit [42].

In de Sitter space, unitarity forbids the mass of the spin-2 field to be arbitrarily small. The mass has to satisfy the Higuchi bound [43, 44]

$$m_{\text{FP}}^2 \geq \frac{2}{3} \Lambda, \quad (2.19)$$

in order to ensure that the helicity-0 mode of the massive spin 2-field is not a ghost state (Higuchi ghost) in the sense that its kinetic term has the correct sign.

3 Background cosmology

3.1 Flat FLRW Ansatz

After having introduced bimetric theory and discussed vacuum solutions we now consider cosmological solutions. Following the cosmological principle, we assume spacetime to be homogenous and isotropic on large scales and spatially flat. Both metrics assume the flat FLRW form,

$$ds_g^2 = -dt^2 + a(t)^2 dx^2, \quad (3.1)$$

$$ds_f^2 = -X(t)^2 dt^2 + b(t)^2 dx^2, \quad (3.2)$$

where a and b are the scale factors of the metric $g_{\mu\nu}$ and $f_{\mu\nu}$ resp., and X is the lapse of the metric $f_{\mu\nu}$. We used the time reparametrization-invariance already to set the lapse of the metric $g_{\mu\nu}$ to unity. This fixes the gauge completely. From now on we do not explicitly write the time-dependence of the metric functions. For later let us define the ratio of the scale factors and the Hubble rates as

$$y = \frac{b}{a}, \quad H = \frac{\dot{a}}{a}, \quad H_f = \frac{\dot{b}}{Xb}, \quad (3.3)$$

where a dot represents derivative w.r.t. cosmic time t . According to homogeneity and isotropy, we assume the universe to be filled with a perfect fluid with stress-energy tensor

$$T_{\mu\nu} = (\rho_m + p_m)u_\mu u_\nu + p_m g_{\mu\nu}, \quad (3.4)$$

where u_μ is the 4-velocity of the fluid with energy density ρ_m and pressure p_m . The latter quantities are related via the linear equation of state

$$w_m = \frac{p_m}{\rho_m}. \quad (3.5)$$

In this work we are mostly interested in the late-time behavior of the universe and in particular in times after radiation-matter-equality. Later we will set $w_m = 0$ in order to describe non-relativistic matter such as baryons and dark matter.

3.2 Equations of motion

The Bianchi constraint (2.9) on the FLRW ansatz reads

$$\left(\dot{b} - X\dot{a}\right) (\beta_1 + 2\beta_2 y + \beta_3 y^2) = 0. \quad (3.6)$$

There are two branches of solutions. Either one demands the term in the second parentheses to vanish, which forces the ratio of the scale factors to be a constant, i.e. $y = \text{const}$. This algebraic branch is pathological [45, 46] and implies that the mass of the massive spin-2 field is identically zero, cf. eq. (2.17). The other solution is given by demanding the term in the first parentheses to vanish, which reads in terms of the Hubble rates

$$H = yH_f. \quad (3.7)$$

This solution is referred to as dynamical branch on which we will focus for the remainder of the paper.

For the isotropic and homogenous ansatz, the conservation eq. (2.8) reduces to the continuity equation

$$\dot{\rho}_m + 3H(1 + w_m)\rho_m = 0. \quad (3.8)$$

This equation is solved by

$$\rho_m = \rho_{m,0} a^{-3(1+w_m)}, \quad (3.9)$$

where $\rho_{\text{m},0}$ is a constant of integration. The time-time-component of the Einstein field eq. (2.5) for $g_{\mu\nu}$ and $f_{\mu\nu}$ on the dynamical branch read

$$3H^2 = \frac{1}{m_g^2} (\rho_{\text{DE}} + \rho_{\text{m}}) \quad (3.10\text{a})$$

$$3H^2 = \frac{1}{m_g^2} \rho_{\text{pot}}, \quad (3.10\text{b})$$

where we have defined the energy densities coming from the interaction potential as

$$\rho_{\text{DE}} = m_g^2 (\beta_0 + 3\beta_1 y + 3\beta_2 y^2 + \beta_3 y^3), \quad (3.11\text{a})$$

$$\rho_{\text{pot}} = \frac{m_g^2}{\alpha^2 y^2} (\beta_1 y + 3\beta_2 y^2 + 3\beta_3 y^3 + \beta_4 y^4). \quad (3.11\text{b})$$

Both energy densities are time dependent via y . The effect of the interaction potential can be interpreted as dynamical Dark Energy with a non-constant equation of state. The eqs. (3.8), (3.10a) and (3.10b) entirely determine the dynamics; the spatial components of the Einstein field eq. (2.5) do not provide further information.

Combining the modified Friedmann eqs. (3.10a) and (3.10b) yields a quartic polynomial for y ,

$$\alpha^2 \beta_3 y^4 + (3\alpha^2 \beta_2 - \beta_4) y^3 + 3(\alpha^2 \beta_1 - \beta_3) y^2 + \left(\alpha^2 \beta_0 - 3\beta_2 + \frac{\alpha^2}{m_g^2} \rho_{\text{m}} \right) y - \beta_1 = 0, \quad (3.12)$$

which determines y as a function of ρ_{m} . Taking the derivative w.r.t. e -folds $\ln a$ and using the continuity eq. (3.8), we arrive at [16]

$$y' = \frac{3(1 + w_{\text{m}}) \alpha^2 y^2 \rho_{\text{m}} / m_g^2}{\beta_1 - 3\beta_3 y^2 - 2\beta_4 y^3 + 3\alpha^2 y^2 (\beta_1 + 2\beta_2 y + \beta_3 y^2)}, \quad (3.13)$$

where prime denotes derivative with respect to e -folds². y' is only a function of y . The variable y captures the dynamics of the cosmological solutions entirely and has a one-dimensional phase-space.

Note that the exchange symmetry (2.10) on the level of the FLRW background reads

$$y \rightarrow -y, \quad \beta_n \rightarrow (-1)^n \beta_n. \quad (3.14)$$

For arbitrary β_n we can restrict ourselves to solutions with $y > 0$ without loss of generality.

3.3 Finite and infinite branch

As mentioned previously, in the presence of a massive spin 2-field on an (A)dS background, the Higuchi bound (2.19) has to be satisfied in order to ensure unitarity. Despite the group-theoretical origin of this bound which is only well defined on (A)dS or Minkowski, it can be generalized to FLRW space [47]. Demanding the absence of ghosts results in the cosmological stability bound

$$m_{\text{eff}}^2 \geq 2H^2. \quad (3.15)$$

in terms of the effective mass parameter

$$m_{\text{eff}}^2 = \left(1 + \frac{1}{\alpha^2 y^2} \right) y (\beta_1 + 2\beta_2 y + \beta_3 y^2). \quad (3.16)$$

In vacuum with $\rho_{\text{m}} = 0$, i.e. $y = c$ and $H^2 = \Lambda/3$, the cosmological stability bound reduces to the usual Higuchi bound.

²The derivative w.r.t. time t and e -folds $\ln a$ of a quantity A are related as $\dot{A} = HA'$.

We can rewrite eq. (3.13) in terms of the cosmological stability bound as

$$y' = y \frac{(1 + w_m)\rho_m/m_g^2}{m_{\text{eff}}^2 - 2H^2}. \quad (3.17)$$

This allows to read off some important features of cosmological solutions. First of all, $y' = 0$ if $\rho_m = 0$ or $y = 0$. That means, the points $y = 0$ and $\rho_m(y) = 0$ cannot be crossed dynamically. These points separate regions of the phase space of different branches of solutions to eq. (3.12). In particular, the vacuum points $\rho_m(y) = 0$ cannot be crossed dynamically. y approaches a constant value as can be seen from the eq. (3.12) for vanishing matter energy density. From the quartic polynomial (3.12) we can identify two different behaviors of y for early times when the matter energy density is large and classically diverges, $\rho_m \rightarrow \infty$:

1. *Infinite branch*: At early times, y diverges as well. The cosmic evolution starts at $y = \infty$ and as the universe expands, y decreases and finally approaches a constant value $y = c$. This constant corresponds to the highest-lying, strictly positive root of eq. (2.14). Since y decreases in time, it follows that $y' < 0$. Now eq. (3.17) implies that either $m_{\text{eff}}^2 < 2H^2$ or $\rho_m < 0$. Hence, the infinite branch either violates the cosmological stability bound or the matter sector has a negative energy density. This implies that the infinite branch necessarily propagates a ghost [48]; it is an unphysical solution.
2. *Finite branch*: Alternatively, $y \rightarrow 0$ at early times. Then y increases in time until it approaches a constant value $y = c$ in the infinite future, which is the lowest-lying, strictly positive root of eq. (2.14). This implies that $y' > 0$ and due to eq. (3.17) the cosmological stability bound is satisfied. This identifies the finite branch as the only solution to the Friedmann eq. (3.10) that is physical.

Besides the finite and infinite branch, the polynomial (3.12) has up to four solutions. These *exotic branches* however were found to not be consistent [48]. For a detailed discussion on the viability of cosmological solutions although in a different parametrization see Ref. [15]. From now on, we will only focus on a cosmic expansion history on the finite branch.

4 Unique vacuum and physical parametrization of solutions

Our aim in this paper is to use cosmological observables to constrain the physical parameters $\bar{\alpha}$, m_{FP} and Λ . However, these parameters can be defined only on proportional solutions and hence in vacuum, while cosmological observables are entities of solutions with matter source. The idea is to use the asymptotic future of the universe as the vacuum point at which the spin-2 mass m_{FP} , mixing angle $\bar{\alpha}$ and cosmological constant Λ are defined and to impose consistency conditions on the expansion history and the asymptotic vacuum point. This results in a unique relation between the parameters that appear in the action and the physical parameters. In this section we work out this strategy in detail and build up the dictionary between the two different parameterizations.

4.1 Rescaling invariance and natural parameter values

The action (2.1) has seven free parameters $\{m_g, \alpha, \beta_n\}$. Due to the properties of the elementary symmetric polynomials that appear in the bimetric potential (2.2), the action is invariant under the combined rescaling

$$f_{\mu\nu} \rightarrow \tilde{f}_{\mu\nu} = \lambda^{-1} f_{\mu\nu}, \quad \alpha \rightarrow \tilde{\alpha} = \lambda^{1/2} \alpha, \quad \beta_n \rightarrow \tilde{\beta}_n = \lambda^{n/2} \beta_n, \quad (4.1)$$

where λ is a constant parameter. On proportional background solutions, the rescaling of the metric $f_{\mu\nu}$ translates into

$$c \rightarrow \tilde{c} = \lambda^{-1/2} c. \quad (4.2)$$

This implies that one of the eight parameters $\{m_g, \alpha, c, \beta_n\}$ is redundant. In order to remove the redundancy from the parameter space, the rescaling has often been used to either set $\tilde{\alpha} = 1$ by choosing $\lambda = \alpha^{-2}$ or to set $\tilde{c} = 1$ by choosing $\lambda = c^2$ in the literature. Let us call this choice to fix the redundancy *rescaled parametrization*. Although being consistent, this choice leads to a very specific region of the bimetric parameter space, in which certain features of bimetric theory are not obvious. This becomes particularly important when studying limits of the theory such as the GR-limit or the massive gravity limit. Suppose, the interaction parameters are all of the same order, $\beta_n \sim \mathcal{O}(m^2)$ where m is some mass scale, e.g. $m = H_0$. Using the rescaling invariance to set $\tilde{\alpha} = 1$, the interaction parameters in rescaled parametrization are of the order $\tilde{\beta}_n \sim \alpha^{-n} \mathcal{O}(m^2)$. In the GR-limit of the theory $\alpha \ll 1$, the rescaled interaction parameters are no longer of the same order. Instead, there is a huge hierarchy between them, $\tilde{\beta}_n \ll \tilde{\beta}_{n+1}$. When working in rescaled parametrization one has to impose a large hierarchy between the interaction parameters in order to arrive at the GR-limit of bimetric theory. At first glance, such a parameter choice appears unnatural which led to confusion in the past on the phenomenological viability of bimetric theory [42].

As shown in Ref. [19], solutions to the bimetric field equations exhibit another GR-limit. If the massive spin 2-field is heavy, $m_{\text{FP}}^2 \gg \Lambda$, the laws of GR are recovered. In order to achieve a large Fierz-Pauli mass by keeping the cosmological constant small requires a large amount of tuning among the interaction parameters β_n . Although this tuning appears to be unnatural, it is another artifact of the rescaling.

To see that, let us briefly discuss the relation between the different parameters without rescaling. First, quantities like the Fierz-Pauli mass and the cosmological constant are defined in proportional background solutions, labeled by the roots c of eq. (2.14). For a generic model, we can distinguish two types of roots by their asymptotic behavior:

- singular root: $c \sim \alpha^{-1}$ as $\alpha \ll 1$
- constant root: c constant as $\alpha \ll 1$.

For both types of roots, the Fierz-Pauli mass becomes large in the limit $\alpha \ll 1$ if we do not tune the β_n . On a singular root, however, the cosmological constant is large as well for $\alpha \ll 1$. In order to achieve the hierarchy on a singular root, one has to tune one of the interaction parameters β_n . On a constant root however, the value of c is such that the cosmological constant is independent of α and of the order of the β_n in the limit, as can be seen from eq. (2.13a). Summarizing, $\alpha \ll 1$ automatically implies $m_{\text{FP}}^2 \gg \Lambda$ without further tuning the interaction parameters on a constant root. Alternatively, one can achieve a large Fierz-Pauli mass, $m_{\text{FP}}^2 \gg \Lambda$, even though α is not small by tuning the interaction parameters β_n (and vice versa). In fact, α and m_{FP} are completely independent of each other if one accepts tuning among the interaction parameters³. We demonstrate this point for a concrete example in appendix A.

4.2 Definition of physical parameters

In this paper, we are seeking a parametrization of solutions to the bimetric field equations that avoids the redundancy due to the rescaling invariance (4.1) and circumvents the aforementioned difficulties that come along with fixing the redundancy by hand. Our proposal is to not work in terms of the parameters of the theory $\{\alpha, \beta_n\}$ as independent parameter, but a different set of parameters, that (a) are invariant under the rescaling (4.1) and (b) have a direct physical interpretation and capture the relevant limits of bimetric theory. These independent parameters are:

- mixing angle: $\bar{\alpha} = \alpha c$,
- Fierz-Pauli mass: m_{FP} ,
- effective cosmological constant: Λ .

³For the question of naturalness of such tuning, we refer to Refs. [29, 49, 50] which studied the quantum corrections coming from matter and graviton loops that the bimetric potential receives.

Those are the *physical parameters* that can be measured by local experiments. If there are three free interaction parameters β_n , all three physical parameters are independent. If there are less, the physical parameters are not independent of each other. For four or five free interaction parameters, we additionally introduce the

- invariant interaction parameters: $\bar{\beta}_n = \alpha^{-n} \beta_n$.

This completes our list of quantities in *physical parametrization*. We treat the physical parameters as independent variables and are agnostic to the underlying values of the parameters of the theory. Instead, the parameters that appear in the action, are functions of the physical quantities, $\alpha = \alpha(\bar{\alpha}, m_{\text{FP}}, \Lambda, \bar{\beta}_n)$ and $\beta_n = \beta_n(\bar{\alpha}, m_{\text{FP}}, \Lambda, \bar{\beta}_n)$.

The physical parametrization comes with its own drawbacks. The physical parameters are parameters of a particular solution, but they are not parameters of the theory. The relation between the theory and physical parameters is ambiguous. The background eq. (2.14) is a polynomial in c of degree 4. It has up to four real-valued roots, c_i . Each root describes a vacuum of bimetric theory and hence c_i labels vacua. Each vacuum is characterized by its own mixing angle $\bar{\alpha}(c_i)$, spin 2-mass $m_{\text{FP}}(c_i)$, and cosmological constant $\Lambda(c_i)$. In other words, for a given set of theory parameters $\{\alpha, \beta_n\}$ there are up to four different sets of physical parameters. However, as it turns out there is only a single consistent vacuum out of the four vacuum solutions. Restricting ourselves to the consistent vacuum implies a unique relation between the theory and physical parameters. We will discuss this point in detail in the following and thereby define what we mean by consistent vacuum. We work out the dictionary between theory and physical parameters model by model in section 5 and appendix B.

4.3 Consistent vacuum

Not every vacuum solution is consistent for a given set of theory parameters $\{\alpha, \beta_n\}$. First of all, we restrict ourselves to positive roots of eq. (2.14),

$$c > 0, \quad (4.3)$$

in order to remove the previously mentioned redundancy from the solution space. Then, a consistent vacuum propagates a massive spin-2 field with a positive Fierz-Pauli mass,

$$m_{\text{FP}} > 0. \quad (4.4)$$

We are only interested in vacua with a positive cosmological constant, i.e. in de Sitter vacua,

$$\Lambda > 0, \quad (4.5)$$

although this is not a theoretical consistency requirement. Finally, the Higuchi bound [43, 44] must be satisfied,

$$m_{\text{FP}}^2 \geq \frac{2}{3} \Lambda, \quad (4.6)$$

for a physical solution.

Besides satisfying these criteria, the physical de Sitter vacuum must be the asymptotic future of the universe. Since only the finite branch gives rise to a viable expansion history, we demand that the consistent vacuum corresponds to the final point of the cosmic evolution along the finite branch. The scale factor ratio y smoothly evolves from zero in the asymptotic past to a constant value in the asymptotic future when $\rho_m \rightarrow 0$. Hence, the asymptotic future is the lowest-lying, strictly positive root of eq. (2.14). This uniquely determines the true vacuum of bimetric theory. The existence and consistency of the finite branch imposes another constraint on the theory parameters. At early times, y approaches zero and the Hubble rate diverges as the matter energy density diverges. From the $f_{\mu\nu}$ -Friedmann eq. (3.10b) we find that $H^2 \rightarrow \infty$ as $y \rightarrow 0$ for $y > 0$ only if [15]

$$\beta_1 > 0. \quad (4.7)$$

This translates into another consistency constraint on the physical parameters.

Summarizing, for a given set of theory parameters we define a vacuum point to be consistent if it is the lowest lying, strictly positive root of eq. (2.14) and satisfies the criteria eqs. (4.3) to (4.7).

The previously described procedure identifies the unique consistent vacuum of bimetric theory for a given set of theory parameters. Once having identified the consistent vacuum, we use eqs. (2.13) and (2.17) to express the theory parameters $\{\alpha, \beta_n\}$ in terms of the physical parameters $\{\bar{\alpha}, m_{\text{FP}}, \Lambda\}$. It allows to rewrite the Friedmann equation and related cosmological quantities in terms of physical parameters, which then can be constrained by cosmological data. We will work out the dictionary in section 5 and appendix B and use it to constrain the physical parameter space with supernovae data in section 6.

4.4 GR- and massive gravity limit in physical parametrization

Let us briefly comment on the limits in physical parametrization in which either General Relativity or Massive Gravity is recovered.

As derived in Refs. [19, 42] and applied to concrete examples in Ref. [24], bimetric solutions have two independent parameter regimes in which the laws of GR are recovered:

1. $\bar{\alpha} \ll 1$,
2. $m_{\text{FP}} \gg \ell^{-1}$,

where ℓ is some typical length scale of the system, e.g. $\ell = \Lambda^{-1/2}$. In the limit of small mixing angle, the fluctuations of the physical metric is aligned with the massless mode, $\delta g_{\mu\nu} \simeq \delta G_{\mu\nu}$. On the other hand, the fluctuations of the auxiliary metric is aligned with the massive mode $\delta f_{\mu\nu} \simeq \delta M_{\mu\nu}$.

The massive gravity limit is arrived at by taking $\bar{\alpha} \gg 1$ as then the metric fluctuation is aligned with the massive fluctuations, $\delta g_{\mu\nu} \simeq \delta M_{\mu\nu}$. In this limit, the gravitational force between two test particles is mediated by the massive spin-2 field only, which gives rise to a Yukawa-type gravitational potential, cf. e.g. Refs. [22, 51, 52]. This limit of the parameter space of bimetric theory is highly constrained by observational data [53].

5 Model-specific considerations

After having established the physical parametrization, we will now explicitly identify the consistent de Sitter vacuum and the resulting relation between the theory and physical parameters for various (sub-)models of bimetric theory. We restrict our analysis to those models where we can identify the unique consistent vacuum for generic theory parameters. These are all bimetric models with up to three non-vanishing interaction parameters. The reader mostly interested in the constraints from cosmological data on the physical parameter space might want to jump to the next section.

Since the polynomial structure of the background eq. (2.14) and the quartic eq. (3.12) differ from model to model, we did not find a unified treatment to discuss a generic model. The following procedure applies to models with at least two non-vanishing interaction parameters; the model(s) with only one non-vanishing interaction parameter will be discussed separately. The recipe goes as follows:

1. Replace two interaction parameters β_n by the physical quantities m_{FP} and Λ using eqs. (2.13) and (2.17).
2. Solve the background eq. (2.14) for the quantity $\bar{\alpha} = \alpha c$ in terms of the physical quantities and the remaining interaction parameters $\bar{\beta}_n = \alpha^{-n} \beta_n$. Each $\bar{\alpha}$ represents a vacuum of the model.
3. Select those vacua $\bar{\alpha}$ that satisfy the consistency conditions in eqs. (4.3) to (4.7). For each set of parameters, pick the lowest-lying strictly positive root $\bar{\alpha}$.
4. For each consistent vacuum, invert the expression for $\bar{\alpha} = \bar{\alpha}(m_{\text{FP}}, \Lambda, \bar{\beta}_n)$ to express one of the remaining interaction parameters in terms of physical parameters. Plug the result into the other expressions.

5. From the requirement $\beta_1 > 0$ find further constraints on the physical parameters.
6. Solve eq. (3.12) for $\rho_m(y)$ and identify the parameter region where $\rho_m \rightarrow 0$ as $\alpha y \rightarrow \bar{\alpha}$ for $\alpha y < \bar{\alpha}$. This ensures that y' does not diverge on the finite branch.

This procedure identifies those parameter ranges in which a viable finite branch exists with a consistent vacuum as the asymptotic future. Moreover, it replaces three theory parameters by physical parameters. Friedmann's equation and all other observables depend only on manifestly rescaling-invariant parameter combination (e.g. $\beta_n y^n$).

For later use, let us introduce the parameters

$$\Omega_{\text{DE}} = \frac{\rho_{\text{DE}}}{3H^2 m_g^2}, \quad \Omega_{\text{m}} = \frac{\rho_{\text{m}}}{3H^2 m_g^2}, \quad \Omega_{\Lambda} = \frac{\Lambda}{3H^2}, \quad \Omega_{\text{FP}} = \frac{m_{\text{FP}}^2}{3H^2}, \quad B_n = \frac{\alpha^{-n} \beta_n}{3H^2} \quad (5.1)$$

inspired by the standard energy density parameters. Note that Λ is the cosmological constant in the asymptotic future. The GR-relation $1 = \Omega_{\Lambda} + \Omega_{\text{m}}$ does not hold in bimetric theory. Instead, the bimetric Friedmann equation can be written as

$$1 = \Omega_{\text{DE}} + \Omega_{\text{m}}. \quad (5.2)$$

The parameter Ω_{DE} describes the energy density that originates from the bimetric potential and is a complicated function of time and the other bimetric parameters. While Ω_{Λ} , Ω_{FP} are time-dependent only via H , the time evolution of the matter energy density is standard,

$$\Omega_{\text{m}} = \frac{H_0^2}{H^2} \Omega_{\text{m},0} (1+z)^{3(1+w_{\text{m}})} \quad (5.3)$$

where the redshift z is related to the scale factor of the physical metric $g_{\mu\nu}$ in the standard way as $a = (z+1)^{-1}$, cf. eq. (3.9). Evaluating the Friedmann equation today yields

$$\Omega_{\text{m},0} = 1 - \Omega_{\text{DE},0}. \quad (5.4)$$

We can use this relation in order to remove one parameter from the Friedmann equation. However, the precise relation between $\Omega_{\text{m},0}$, $\Omega_{\Lambda,0}$, $\Omega_{\text{FP},0}$, $\bar{\alpha}$, and $B_{n,0}$ depends on the model.

In the remainder of this section, we will discuss several (sub-)models of bimetric theory and build up the dictionary between the theory and physical parameters. We complete the dictionary for the three parameter models in appendix B.

5.1 1-parameter model: β_1 -model

As a warm-up let us first discuss the one parameter models in order to demonstrate the procedure. The only one parameter model that can possibly give rise to a viable expansion history is the β_1 -model. With only one interaction parameter being non-zero, the parameter space is highly restricted and the physical parameters are not independent. Instead, eqs. (2.13), (2.14) and (2.17) imply

$$\bar{\alpha}^2 = \frac{1}{3}, \quad m_{\text{FP}}^2 = \frac{4}{3}\Lambda. \quad (5.5)$$

The model has two vacua, $\bar{\alpha}_{\pm} = \pm \frac{1}{\sqrt{3}}$. Both vacua satisfy the Higuchi bound, but only $\bar{\alpha}_+$ is strictly positive. The interaction parameter is given by $\alpha^{-1}\beta_1 = \Lambda/(3\bar{\alpha})$, which is manifestly positive on the positive vacuum as desired. Thus, we identified the unique consistent vacuum of the β_1 -model. Note that $\bar{\alpha}$ is constant and not a free parameter. Both vacua of the β_1 -model do not have a GR- or massive gravity limit.

Next, we study the finite branch of the FLRW solution. The quartic eq. (3.12) has two solutions for y ,

$$\bar{y}_{\pm} = \frac{\pm \sqrt{4\Lambda + \frac{\rho_{\text{m}}^2}{m_{\text{g}}^4} - \frac{\rho_{\text{m}}}{m_{\text{g}}^2}}}{2\sqrt{3}\Lambda}, \quad (5.6)$$

of which \bar{y}_+ corresponds to the finite branch as can be seen from the limits of large and small ρ_m . Now we explicitly see that $\bar{y}_\pm \rightarrow \bar{\alpha}_\pm$ in the asymptotic future. Plugging y_+ into the modified Friedmann eq. (3.10a) gives

$$3H^2 = \frac{\rho_m}{2m_g^2} + \sqrt{\Lambda^2 + \frac{\rho_m^2}{4m_g^4}}. \quad (5.7)$$

With the Friedmann equation in this parametrization, we can use cosmological observables to constrain the physical parameters.

Rewriting the modified Friedmann eq. in terms of the parameters in (5.1) yields

$$2 = \Omega_m + \sqrt{\Omega_m^2 + 4\Omega_\Lambda^2} \quad (5.8)$$

Evaluating the Friedmann equation today at redshift $z = 0$ yields the relation

$$\Omega_{\Lambda,0} = \sqrt{1 - \Omega_{m,0}}. \quad (5.9)$$

This implies, that the contribution from the bimetric potential today reads $\Omega_{\text{DE},0} = \Omega_{\Lambda,0}^2$. Now we have all the ingredients to finally compare the model to cosmological data. This will be done in the next section.

5.2 2-parameter models

Let us discuss models with two interaction parameters being non-zero. Since β_1 must be non-zero for the existence of the finite branch, we are left with four 2-parameter models that can possibly give rise to a viable expansion history: $\beta_0\beta_1$, $\beta_1\beta_2$, $\beta_1\beta_3$, and $\beta_1\beta_4$. Only two of the three physical parameters are independent. In fig. 1 we show how $\bar{\alpha}$ depends on m_{FP}^2/Λ , which we derive in the following subsections. Note already, that only for the $\beta_0\beta_1$ -model, the parameter $\bar{\alpha}$ has a range from zero to infinity. For the other two parameter models, $\bar{\alpha} < 1$ always. This becomes clear when working out the precise relation between the physical parameters.

The dependency among the physical parameters has important consequences for the existence of a well-defined GR-limit and massive gravity (MG) limit. The β_1 -model does not have a GR- or MG-limit at all because $\bar{\alpha}$ is fixed by the equations of motion to a constant value. For the $\beta_0\beta_1$ -model, the GR-limit is arrived at by taking $m_{\text{FP}}^2 = \Lambda$, while the MG-limit is arrived at by $m_{\text{FP}}^2 \gg \Lambda$. For the other two parameter models the situation is different, where the GR-limit is characterized by $m_{\text{FP}}^2 \gg \Lambda$, while they do not have a consistent MG-limit. Only for the $\beta_1\beta_4$ -model, in principle one can achieve $\bar{\alpha} \gg 1$ by taking $m_{\text{FP}}^2 = \Lambda/3$, which however violates the Higuchi bound. Summarizing, of the 1- and 2-parameter models, only the $\beta_0\beta_1$ -model has a consistent massive gravity limit. This can be seen from fig. 1 and the precise relations that we derive in the following subsections. The GR- and MG-limits are summarized in table 1.

After this summary, let us apply the procedure introduced earlier in order to express the interaction parameters in terms of physical parameters.

5.2.1 $\beta_0\beta_1$ -model

We start by analysing the model with $\beta_2 = \beta_3 = \beta_4 = 0$. Solving the background equations eqs. (2.13), (2.14) and (2.17) yields

$$\bar{\alpha}_\pm = \pm \sqrt{\frac{m_{\text{FP}}^2}{\Lambda} - 1} \quad (5.10a)$$

$$\beta_0 = -3m_{\text{FP}}^2 + 4\Lambda, \quad (5.10b)$$

$$\alpha^{-1}\beta_1 = \pm \sqrt{(m_{\text{FP}}^2 - \Lambda)\Lambda}. \quad (5.10c)$$

Only in the parameter range

$$m_{\text{FP}}^2 > \Lambda, \quad (5.11)$$

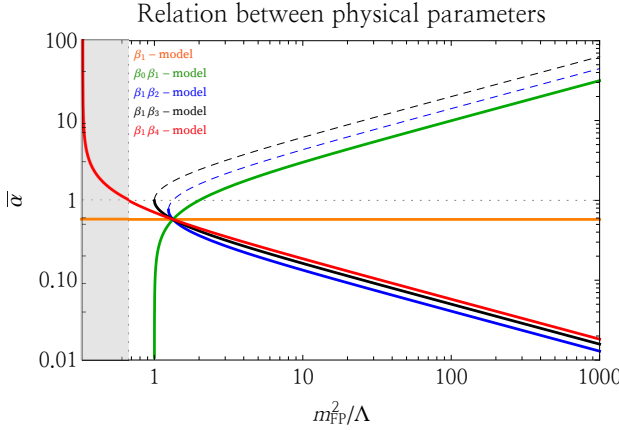


Figure 1: This figure shows the relation between $\bar{\alpha}$ and m_{FP}^2/Λ for the 1- and 2-parameter models on the consistent vacuum. The dashed lines correspond to the highest-lying, strictly positive root of the model. In the gray-shaded region the Higuchi bound is violated.

Model	GR limit	MG limit
β_1	–	–
$\beta_0\beta_1$	$m_{\text{FP}}^2 = \Lambda$	$m_{\text{FP}}^2 \gg \Lambda$
$\beta_1\beta_2$	$m_{\text{FP}}^2 \gg \Lambda$	–
$\beta_1\beta_3$	$m_{\text{FP}}^2 \gg \Lambda$	–
$\beta_1\beta_4$	$m_{\text{FP}}^2 \gg \Lambda$	$(m_{\text{FP}}^2 = \Lambda/3)$

Table 1: Summary of the general relativity (GR) limit $\bar{\alpha} \ll 1$ and the massive gravity (MG) limit $\bar{\alpha} \gg 1$ for the one and two parameter models. A – indicates that the limit is not consistent.

the vacuum points and β_1 are real-valued. This bound is more restrictive than the Higuchi bound. In the same parameter range, only the vacuum point $\bar{\alpha}_+$ is strictly positive and hence we discard $\bar{\alpha}_-$. This uniquely identifies $\bar{\alpha}_+$ as the consistent de Sitter vacuum of the $\beta_0\beta_1$ model.

Next, we find the roots of eq. (3.12) of which only one describes a consistent finite branch. Plugging the result into eq. (3.10a) and using eqs. (5.1) and (5.10) yields the modified Friedmann equation

$$2 = -3\Omega_{\text{FP}} + 4\Omega_{\Lambda} + \Omega_{\text{m}} + \sqrt{(3\Omega_{\text{FP}} - 2\Omega_{\Lambda})^2 + 2(-\Omega_{\text{FP}} + 4\Omega_{\Lambda})\Omega_{\text{m}} + \Omega_{\text{m}}^2}. \quad (5.12)$$

Evaluating the Friedmann equation today implies

$$\Omega_{\text{FP},0} = \Omega_{\Lambda,0} - \frac{1}{3} + \frac{\Omega_{\text{m},0}}{3 - 3\Omega_{\Lambda,0}}, \quad (5.13)$$

which allows to eliminate one of the parameters. Consistency requires $\Omega_{\text{FP},0} > \Omega_{\Lambda,0}$ and $\Omega_{\text{FP},0} > 0$, which translates into

$$\Omega_{\Lambda,0} > 1 - \Omega_{\text{m},0} \quad (5.14)$$

$$\Omega_{\Lambda,0} > \frac{2 - \sqrt{1 + 3\Omega_{\text{m},0}}}{3}. \quad (5.15)$$

This completes the dictionary for the $\beta_0\beta_1$ model.

5.2.2 $\beta_1\beta_2$ -model

Next, we consider the model with $\beta_0 = \beta_3 = \beta_4 = 0$. In physical parametrization, the background eq. (2.14) has four roots. The two solutions with $\bar{\alpha} > 0$ are

$$\bar{\alpha}_{\pm} = \sqrt{\frac{3m_{\text{FP}}^2 - 2\Lambda \pm \sqrt{9m_{\text{FP}}^4 - 12m_{\text{FP}}^2\Lambda + \Lambda^2}}{3\Lambda}}, \quad (5.16a)$$

$$\alpha^{-1}\beta_{1\pm} = \frac{\bar{\alpha}_{\pm}}{2} \left(3m_{\text{FP}}^2 - 3\Lambda \mp \sqrt{9m_{\text{FP}}^4 - 12m_{\text{FP}}^2\Lambda + \Lambda^2} \right), \quad (5.16b)$$

$$\alpha^{-2}\beta_{2\pm} = -\frac{1}{6} \left(3m_{\text{FP}}^2 - 5\Lambda \mp \sqrt{9m_{\text{FP}}^4 - 12m_{\text{FP}}^2\Lambda + \Lambda^2} \right). \quad (5.16c)$$

The other two roots are given by $-\bar{\alpha}_\pm$, but we discard them due to our requirement $\bar{\alpha} > 0$. Both, $\bar{\alpha}_\pm$ and the interaction parameters are real-valued and positive only in the parameter range

$$m_{\text{FP}}^2 > \frac{2 + \sqrt{3}}{3} \Lambda, \quad (5.17)$$

which is more restrictive than the Higuchi bound. In the same parameter range, we find that $\bar{\alpha}_- < \bar{\alpha}_+$. This identifies $\bar{\alpha}_-$ as the lowest-lying strictly positive root and thus the unique consistent vacuum of the $\beta_1\beta_2$ model. Therefore, we use β_{1-} and β_{2-} in order to replace interaction parameters by physical parameters.

The polynomial (3.12) has degree 3 and hence there are up to three real-valued roots y . The explicit expressions are lengthy and not enlightening so we do not write them here. Instead, we only report the result from evaluating the Friedmann equation today. The relation between the parameters reads

$$\begin{aligned} \Omega_{\text{m},0} = & \frac{(\Omega_{\Lambda,0} - 1)}{(2 + 6\Omega_{\text{FP},0} - 10\Omega_{\Lambda,0} - 9\Omega_{\text{FP},0}\Omega_{\Lambda,0} + 12\Omega_{\Lambda,0}^2)^2} \left[-27\Omega_{\text{FP},0}^3\Omega_{\Lambda,0} \right. \\ & + 9\Omega_{\text{FP},0}^2(4 + 17\Omega_{\Lambda,0}^2 + \Omega_{\Lambda,0}(-12 + \sqrt{9\Omega_{\text{FP},0}^2 - 12\Omega_{\text{FP},0}\Omega_{\Lambda,0} + \Omega_{\Lambda,0}^2})) \\ & - 6\Omega_{\text{FP},0}(-4 + 24\Omega_{\Lambda,0} + 43\Omega_{\Lambda,0}^3 + \Omega_{\Lambda,0}^2(-50 + 3\sqrt{9\Omega_{\text{FP},0}^2 - 12\Omega_{\text{FP},0}\Omega_{\Lambda,0} + \Omega_{\Lambda,0}^2})) \\ & + 2\left(2 + 68\Omega_{\Lambda,0}^4 - \Omega_{\Lambda,0}(18 + \sqrt{9\Omega_{\text{FP},0}^2 - 12\Omega_{\text{FP},0}\Omega_{\Lambda,0} + \Omega_{\Lambda,0}^2}) + \Omega_{\Lambda,0}^2(63 + \sqrt{9\Omega_{\text{FP},0}^2 - 12\Omega_{\text{FP},0}\Omega_{\Lambda,0} + \Omega_{\Lambda,0}^2}) \right. \\ & \left. \left. + \Omega_{\Lambda,0}^3(-103 + 4\sqrt{9\Omega_{\text{FP},0}^2 - 12\Omega_{\text{FP},0}\Omega_{\Lambda,0} + \Omega_{\Lambda,0}^2}) \right) \right] \quad (5.18) \end{aligned}$$

These are all the ingredients that we need for the data analysis.

5.2.3 $\beta_1\beta_3$ -model

The $\beta_1\beta_3$ model is defined by $\beta_0 = \beta_2 = \beta_4 = 0$. The background eqs. (2.13), (2.14) and (2.17) have the following solutions,

$$\bar{\alpha}_\pm = \sqrt{\frac{2m_{\text{FP}}^2 - \Lambda \pm 2m_{\text{FP}}\sqrt{m_{\text{FP}}^2 - \Lambda}}{\Lambda}}, \quad (5.19a)$$

$$\alpha^{-1}\beta_{1\pm} = \frac{\bar{\alpha}^\pm}{4} \sqrt{3m_{\text{FP}}^2 - 2\Lambda \mp 3m_{\text{FP}}\sqrt{m_{\text{FP}}^2 - \Lambda}}, \quad (5.19b)$$

$$\alpha^{-3}\beta_{3\pm} = -\bar{\alpha}^\pm \left(4m_{\text{FP}}^4 - 7m_{\text{FP}}^2\Lambda + 2\Lambda^2 \mp \sqrt{m_{\text{FP}}^2 - \Lambda}(4m_{\text{FP}}^2 - 5\Lambda)m_{\text{FP}} \right). \quad (5.19c)$$

We find that $\bar{\alpha}_\pm$, $\beta_{1\pm}$, and $\beta_{3\pm}$ are positive and real-valued only in the parameter range ⁴

$$m_{\text{FP}}^2 > \Lambda, \quad (5.20)$$

which is more restrictive than the Higuchi bound. In the same parameter region we find that $\bar{\alpha}_- < \bar{\alpha}_+$. This identifies $\bar{\alpha}_-$ as the unique consistent vacuum.

⁴Strictly speaking, β_{1+} is positive and real-valued only in the parameter range $\frac{3}{4}m_{\text{FP}}^2 < \Lambda < m_{\text{FP}}^2$. However, $\bar{\alpha}_+$ is not a consistent vacuum point anyways.

Evaluating the Friedmann equation for $z = 0$ implies the following relation among the energy density parameters,

$$\begin{aligned} \Omega_{\text{m},0} = & \frac{2\Omega_{\Lambda,0}^2}{27(-2\Omega_{\text{FP},0} + \Omega_{\Lambda,0} + 2\sqrt{\Omega_{\text{FP},0}(\Omega_{\text{FP},0} + \Omega_{\Lambda,0})})} \left[-108\Omega_{\text{FP},0} - 108\sqrt{\Omega_{\text{FP},0}^5(\Omega_{\text{FP},0} - \Omega_{\Lambda,0})} + 297\Omega_{\text{FP},0}^2\Omega_{\Lambda,0} \right. \\ & + 243\sqrt{\Omega_{\text{FP},0}^3(\Omega_{\text{FP},0} - \Omega_{\Lambda,0})}\Omega_{\Lambda,0} - 243\Omega_{\text{FP},0}\Omega_{\Lambda,0}^2 + 2\Omega_{\Lambda,0} \left(2 + 9\Omega_{\Lambda,0} \left(2\Omega_{\Lambda,0} - 7\sqrt{\Omega_{\text{FP},0}(\Omega_{\text{FP},0} - \Omega_{\Lambda,0})} \right) \right) \\ & \left. + \Omega_{\Lambda,0} \left(-2 + 18\Omega_{\text{FP},0}^2 + 18\sqrt{\Omega_{\text{FP},0}^3(\Omega_{\text{FP},0} - \Omega_{\Lambda,0})} - 33\Omega_{\text{FP},0}\Omega_{\Lambda,0} + 12\Omega_{\Lambda,0} \left(\Omega_{\Lambda,0} - 2\sqrt{\Omega_{\text{FP},0}(\Omega_{\text{FP},0} - \Omega_{\Lambda,0})} \right) \right) \right) \\ & \times \sqrt{4 + 18\Omega_{\text{FP},0}^2 + 18\sqrt{\Omega_{\text{FP},0}^3(\Omega_{\text{FP},0} - \Omega_{\Lambda,0})} - 33\Omega_{\text{FP},0}\Omega_{\Lambda,0} + 12\Omega_{\Lambda,0} \left(\Omega_{\Lambda,0} - 2\sqrt{\Omega_{\text{FP},0}(\Omega_{\text{FP},0} - \Omega_{\Lambda,0})} \right)} \Big], \end{aligned} \quad (5.21)$$

which agrees with the relation given in Ref. [15], as we checked explicitly. Since the expressions are too lengthy, we do not show the Friedmann equation on the finite branch in full glory.

5.2.4 $\beta_1\beta_4$ -model

Finally, we discuss the $\beta_1\beta_4$ -model which is defined by setting $\beta_0 = \beta_2 = \beta_3 = 0$. The background eqs. (2.13), (2.14) and (2.17) have the following roots,

$$\bar{\alpha}_{\pm} = \pm \sqrt{\frac{\Lambda}{3m_{\text{FP}}^2 - \Lambda}}, \quad (5.22a)$$

$$\alpha^{-1}\beta_{1\pm} = \frac{1}{3}\sqrt{(3m_{\text{FP}}^2 - \Lambda)\Lambda}, \quad (5.22b)$$

$$\alpha^{-4}\beta_{4\pm} = -\frac{9m_{\text{FP}}^4 - 15m_{\text{FP}}^2\Lambda + 4\Lambda^2}{3\Lambda}. \quad (5.22c)$$

The roots are real-valued in the parameter range $3m_{\text{FP}}^2 > \Lambda$, which is less restrictive than the Higuchi bound. In the consistent parameter range, only the root $\bar{\alpha}_+$ is strictly positive. This identifies $\bar{\alpha}_+$ as the unique consistent vacuum of the $\beta_1\beta_4$ model. When the Higuchi bound is satisfied, also the interaction parameter β_{1+} is positive.

Instead of presenting the lengthy expression for the Friedmann equation on the finite branch, we only evaluate it today. The resulting relation among the parameters is

$$\Omega_{\text{FP},0} = \frac{\Omega_{\Lambda,0}(-4 + 12\Omega_{\text{m},0} - 12\Omega_{\text{m},0}^2 + 4\Omega_{\text{m},0}^3 + 3\Omega_{\Lambda,0} - \Omega_{\text{m},0}\Omega_{\Lambda,0} + \Omega_{\Lambda,0}^3)}{3(-1 + 3\Omega_{\text{m},0} - 3\Omega_{\text{m},0}^2 + \Omega_{\text{m},0}^3 + \Omega_{\Lambda,0}^3)}. \quad (5.23)$$

This completes the dictionary of the 2-parameter models.

5.3 3-parameter models

In this section we will discuss models with three non-vanishing interaction parameters. That means that all three physical parameters $\bar{\alpha}$, m_{FP} , and Λ are independent and not fixed by the background equations. We focus on the two extreme cases: the three parameter model without vacuum energy ($\beta_0 = \beta_4 = 0$) and the model with vacuum energy in both sectors ($\beta_2 = \beta_3 = 0$). We complete the dictionary for the other three parameter models in appendix B.

5.3.1 $\beta_1\beta_2\beta_3$ -model

Following the procedure, there are two positive vacuum points $\bar{\alpha}_{\pm}$. The quartic polynomial (2.14) is solved most easily leaving β_2 as a free parameter. Then the roots take the form

$$\bar{\alpha}_{\pm}^2 = \frac{2m_{\text{FP}}^2 - \Lambda - \bar{\beta}_2 \pm \sqrt{(2m_{\text{FP}}^2 - \bar{\beta}_2)^2 - 4m_{\text{FP}}^2\Lambda}}{2\bar{\beta}_2 + \Lambda}, \quad (5.24)$$

where $\bar{\beta}_2 = \alpha^{-2}\beta_2$. The roots $\bar{\alpha}_\pm$ are real-valued in the following parameter ranges:

$$\bar{\alpha}_+^2 > 0 \iff -\frac{\Lambda}{2} < \bar{\beta}_2 < 2m_{\text{FP}}(m_{\text{FP}} - \sqrt{\Lambda}), \quad (5.25a)$$

$$\bar{\alpha}_-^2 > 0 \iff \bar{\beta}_2 < 2m_{\text{FP}}(m_{\text{FP}} - \sqrt{\Lambda}) \quad (5.25b)$$

We find that $\bar{\alpha}_- < \bar{\alpha}_+$ in the parameter range, where both roots are real-valued. This identifies $\bar{\alpha}_-$ is the lowest-lying, strictly positive root and hence as the unique consistent vacuum of the $\beta_1\beta_2\beta_3$ model. For $\bar{\beta}_2 \rightarrow -\Lambda/2$ we find that $\bar{\alpha}_- \rightarrow \infty$ such that we have to exclude this point.

Solving the expression for $\bar{\alpha}_-$ for β_2 and suppressing the label from now on, we find for the interaction parameters in terms of physical parameters

$$\alpha^{-1}\beta_1 = \frac{-6\bar{\alpha}^2 m_{\text{FP}}^2 + (3 + 4\bar{\alpha}^2 + \bar{\alpha}^4)\Lambda}{4\bar{\alpha}(1 + \bar{\alpha}^2)}, \quad (5.26a)$$

$$\alpha^{-2}\beta_2 = \frac{4\bar{\alpha}^2 m_{\text{FP}}^2 - (1 + \bar{\alpha}^2)^2 \Lambda}{2\bar{\alpha}^2(1 + \bar{\alpha}^2)}, \quad (5.26b)$$

$$\alpha^{-3}\beta_3 = \frac{(1 + 3\bar{\alpha}^4)\Lambda - \bar{\alpha}^2(6m_{\text{FP}}^2 - 4\Lambda)}{4\bar{\alpha}^3(1 + \bar{\alpha}^2)}, \quad (5.26c)$$

where the simplified expressions for β_1 and β_3 are only valid in the parameter range eq. (5.27b). The constraints on the interaction parameter β_2 translate as follows,

$$\bar{\beta}_2 \neq -\frac{\Lambda}{2} \implies m_{\text{FP}}^2 \neq \frac{(1 + \bar{\alpha}^2)\Lambda}{4\bar{\alpha}^2}, \quad (5.27a)$$

$$\bar{\beta}_2 < 2m_{\text{FP}}(m_{\text{FP}} - \sqrt{\Lambda}) \implies m_{\text{FP}}^2 < \frac{(1 + \bar{\alpha}^2)^2 \Lambda}{4\bar{\alpha}^4}. \quad (5.27b)$$

Outside these parameter regions the vacuum $\bar{\alpha}_-$ is not well-defined and they have to be excluded from the parameter space⁵. In fig. 2, the first bound is represented by the blue-dashed line, while the second bound is indicated by the blue-shaded region. On the vacuum point $\bar{\alpha}_-$, $\beta_1 > 0$ is satisfied in the parameter ranges⁶

$$(1) \quad m_{\text{FP}}^2 > \frac{(3 + 2\bar{\alpha}^2 - \bar{\alpha}^4)}{12(1 - \bar{\alpha}^2)} \Lambda \quad \text{for } \bar{\alpha} \geq \frac{\sqrt{\sqrt{33} - 3}}{2}, \quad (5.28a)$$

$$(2) \quad m_{\text{FP}}^2 < \frac{(3 + 4\bar{\alpha}^2 + \bar{\alpha}^4)}{6\bar{\alpha}^2} \Lambda \quad \text{for } \bar{\alpha} < \frac{\sqrt{\sqrt{33} - 3}}{2}. \quad (5.28b)$$

In fig. 2 the red-shaded region indicates where $\beta_1 < 0$. Moving to cosmology, we can expand the quartic polynomial in eq. (3.12) around $y = \bar{\alpha}_-$. We find that ρ_m approaches zero only in the parameter range (5.27b).

Let us summarize the most stringent bounds. The $\beta_1\beta_2\beta_3$ -model can give rise to a consistent expansion history only in the parameter region

$$(1) \quad \frac{m_{\text{FP}}^2}{\Lambda} \leq \frac{(1 + \bar{\alpha}^2)^2}{4\bar{\alpha}^4} \quad \text{for } \bar{\alpha}^2 > \frac{\sqrt{33} - 3}{2}, \quad (5.29a)$$

$$(2) \quad \frac{m_{\text{FP}}^2}{\Lambda} < \frac{(3 + 4\bar{\alpha}^2 + \bar{\alpha}^4)}{6\bar{\alpha}^2} \quad \text{for } \bar{\alpha}^2 < \frac{\sqrt{33} - 3}{2}, \quad (5.29b)$$

$$(3) \quad \frac{m_{\text{FP}}^2}{\Lambda} \neq \frac{1 + \bar{\alpha}^2}{4\bar{\alpha}^2} \quad \text{for any } \bar{\alpha}. \quad (5.29c)$$

⁵Strictly speaking, the condition (5.25) translates into $4\bar{\alpha}^4 m_{\text{FP}}^2 \neq (1 + \bar{\alpha}^2)^2 \Lambda$. However, we find that for $4\bar{\alpha}^4 m_{\text{FP}}^2 > (1 + \bar{\alpha}^2)^2 \Lambda$, the expression for the vacuum point is not invertible. We explicitly checked that in this parameter range, ρ does not vanish at $y = \bar{\alpha}_-/\alpha$. Therefore, we have to exclude this parameter region and this is indicated by the \implies in eq. (5.27).

⁶Note that region (1) is already excluded by eq. (5.27), but we mention it anyways for completeness.

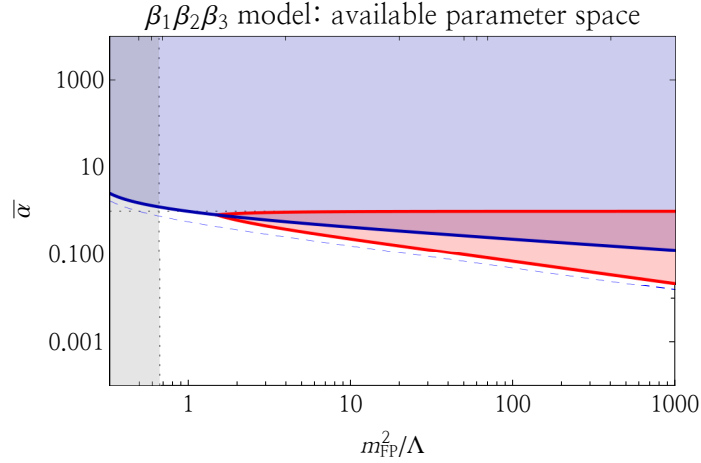


Figure 2: The allowed parameter space in the $\bar{\alpha} - m_{\text{FP}}$ -plane for the $\beta_1\beta_2\beta_3$ -model. The spin-2 mass is given as multiples of the cosmological constant Λ . Within the red-shaded region, the Hubble rate and the energy density are negative at early times because $\beta_1 < 0$, cf. eq. (5.28). In the blue-shaded region, the vacuum point is not well-defined and hence this parameter space is excluded as well, cf. eq. (5.27). The dashed blue line must be excluded, because the parameter replacements are not well-defined, cf. eq. (5.27). A viable finite branch can only exist outside the colored regions. The strongest bounds are summarized in eq. (5.29). Within the gray-shaded region the Higuchi bound is violated.

At the point $\bar{\alpha}^2 = \frac{\sqrt{33}-3}{2}$, the bounds in (1) and (2) coincide with $m_{\text{FP}}^2/\Lambda < (19+3\sqrt{33})/24 \approx 1.5$. The physical parameter space for the three parameter model without bare cosmological constants is highly constrained by theoretical consistency requirements. A large Fierz-Pauli mass is only consistent, if $\bar{\alpha}$ is sufficiently small. Otherwise the vacuum is not consistent. Finally, for large spin 2-masses, the consistency bounds can be summarized as $\bar{\alpha}^2 < \Lambda/(2m_{\text{FP}}^2)$.

5.3.2 $\beta_0\beta_1\beta_4$ -model

After having studied the three parameter model without any bare cosmological constant, we move to the opposite case including vacuum energy for both metrics, the $\beta_0\beta_1\beta_4$ -model. In physical parametrization but leaving β_0 free, this model has two roots, one of which is positive. It is given by

$$\bar{\alpha}^2 = \frac{\Lambda - \beta_0}{3m_{\text{FP}}^2 - \Lambda + \beta_0} \quad (5.30)$$

and well-defined within the parameter range, where $0 < \Lambda - \beta_0 < 3m_{\text{FP}}^2$. This is the unique consistent de Sitter vacuum of the $\beta_0\beta_1\beta_4$ model. Solving this relation for β_0 , we find the interaction parameters in terms of the physical parameters

$$\beta_0 = \frac{\Lambda - \bar{\alpha}^2(3m_{\text{FP}}^2 - \Lambda)}{1 + \bar{\alpha}^2}, \quad (5.31a)$$

$$\alpha^{-1}\beta_1 = \frac{\bar{\alpha}m_{\text{FP}}^2}{1 + \bar{\alpha}^2}, \quad (5.31b)$$

$$\alpha^{-4}\beta_4 = -\frac{m_{\text{FP}}^2 - (1 + \bar{\alpha}^2)\Lambda}{\bar{\alpha}^2(1 + \bar{\alpha}^2)}. \quad (5.31c)$$

This expression for β_0 automatically satisfies the parameter bound above, when the Higuchi bound is satisfied. Also β_1 is manifestly positive. Hence, the replacements above are unique and well-defined for the entire parameter space in which the Higuchi bound is satisfied.

When expanding the quartic polynomial in eq. (3.12) around $y = \bar{\alpha}$ and $y = 0$, we find that the Hubble rate and the energy density are well-behaved in the same parameter region where the physical parameters satisfy the Higuchi bound.

Summarizing, the $\beta_0\beta_1\beta_4$ -model has a well-defined and consistent expansion history and asymptotic de Sitter point as soon as the Higuchi bound is satisfied. This is in stark contrast to the $\beta_1\beta_2\beta_3$ -model where the parameter-space is highly restricted by demanding consistency already. This suggests that the other three parameter models interpolate between these two extreme cases.

6 Constraints from SN1a

In the previous sections we have collected all the ingredients allowing us to finally compare the bimetric (sub)models to real data. We first introduce the observable that provides the data (supernovae) and explain the data analysis. In the last subsection we will summarize and discuss the results.

6.1 Supernovae Type 1a

In this paper, we focus on supernovae of type 1a as cosmological observable. Their luminosity can be determined independently of the redshift which allows to reconstruct the redshift-distance relationship (the Hubble diagram). In 1998, supernovae provided the first evidence that our Universe is currently in a phase of accelerated expansion [54, 55]. Since then, they have become a powerful tool in constraining cosmological parameters of gravitational theories. A gravitational theory like bimetric theory predicts the Hubble rate as a function of redshift z , $H = H(z)$. This allows to calculate various cosmic distances, of which the luminosity distance d_L is the relevant one for supernovae. In terms of the rescaled Hubble parameter $E(z) = H(z)/H_0$ (where $H_0 = H(z=0)$), the luminosity distance reads

$$d_L(z) = \frac{c}{H_0}(1+z) \int_0^z \frac{dz'}{E(z')}. \quad (6.1)$$

Let us already define the rescaled luminosity distance $D_L = H_0 d_L$, which is independent of the value of H_0 . The apparent magnitude is related to the luminosity distance as

$$m = M + 25 + 5 \log_{10} d_L \quad (6.2)$$

where M is the absolute magnitude. This quantity can be compared to the measured magnitude of a supernova.

The data set we are using is the Union2.1 compilation of SN1a as reported in Ref. [56]. It contains 580 supernovae with redshifts up to $z \lesssim 1.4$.

6.2 Data analysis

We aim at constraining the model with real data and thereby finding the regions of the physical parameter space of bimetric theory that is in agreement with observations. We take the Bayesian perspective as it has become standard in cosmology for parameter estimation. Let x be a vector of real data and θ a parameter vector. Bayes inference relies on Bayes' theorem [57]

$$p(\theta|x) = \frac{p(x|\theta)p(\theta)}{p(x)}. \quad (6.3)$$

In observational cosmology the term $p(x)$ is referred to as evidence and is the probability for the observed data x to occur. The evidence appears as an overall normalization and is relevant mostly for model comparison which is not of interest for us in this paper. In order to find the region of the parameter space that is preferred by the data, we have to determine the posterior probability distribution function (PDF), $p(\theta|x)$. It describes the probability for the parameters θ to be the true values given the measured data x . We have to choose priors $p(\theta)$ and calculate the likelihood $\mathcal{L}(\theta) \equiv p(x|\theta)$ which we will describe in the next two sections. Instead of discussing Bayesian inference in further detail, we refer the interested reader to Refs. [58–61].

Within Bayesian statistics there are several methods to scan the parameter space in order to map the posterior PDF. The most straightforward way is to discretize the parameter space and perform a grid scan. On each point of the grid one calculates the likelihood $\mathcal{L}(\theta)$. However, when

implemented numerically this method might be quite slow because computing time is used to evaluate the likelihood in regions of the parameter space where the model does not give a good fit anyways. In addition, we are usually interested in the posterior PDF on a subset of the full parameter space. This marginalization requires integrating the posterior PDF over some directions of the parameter space which might need a lot of computing time. Both drawbacks become particularly relevant when the parameter space is highly dimensional. A more efficient approach is the Markov Chain Monte Carlo (MCMC) method which has become very popular in cosmological data analysis [62, 63]. Of particular interest is the Metropolis-Hastings algorithm which we choose to use for our statistical analysis. It explores the parameter space in regions where the likelihood is large in great detail. It automatically yields the marginal posterior PDFs for each parameter individually as point frequencies of the chains. To ensure that the result of the algorithm maps the posterior PDFs to high precision, i.e. ensuring the Markov chains converge, they have to be long enough. Convergence can be checked, e.g., by comparing several Markov chains that started in different regions of the parameter space. For a chain to be independent of the starting point, a certain amount of steps needs to be removed as a burn-in. The number of chains, length of each chain and number of burn-in steps per chain are a matter of choice. Convergence can only be assessed *a posteriori*. The Gelman-Rubin factor \mathcal{R} [64] provides some quantitative measure of convergence. For more details on MCMCs and their application in cosmology we refer to Refs. [65, 66].

6.2.1 Choice of priors

A key feature in Bayesian inference is the freedom to choose priors $p(\theta)$. Here we can use all the knowledge about the physical parameter space that we have gained in the past. This is the subject of the present section.

Let us start by explicitly stating which are the parameters that we fix to a certain value although most generally they should be subject to the statistical analysis. In that sense, strictly speaking these are not priors. We are interested in times after matter-radiation-equality. Therefore, we assume the matter energy density to be composed of non-relativistic matter (such as baryonic and dark matter) only. We set the energy density of radiation (photons, neutrinos) to zero and the matter equation of state is consequently $w_m = 0$. In addition, we assume the universe to be exactly spatially flat although this conclusion was drawn only in the context of the Λ CDM model. Both these assumptions base their justification on the Λ CDM model. Since this model describes the cosmological data to a high precision and since we expect our models to not deviate too much from the predictions of the Λ CDM model (at least at late times), we believe both assumptions to be justified also within bimetric theory.

Let us move to actual priors. Of course, the energy density parameters should be positive, $\Omega_{m,0} > 0$ and $\Omega_{\Lambda,0} > 0$, as in Λ CDM. In addition, we have defined and derived various consistency conditions for a model to be viable in sections 4 and 5. We use these conditions as priors and accept only those parameter combinations that satisfy all aforementioned conditions. If any of the consistency conditions is violated, we set the prior probability for that parameter combination to zero, and to one otherwise.

These consistency requirements still allow for an infinitely extended parameter space. That is, $\bar{\alpha}$ can range from 0 to infinity. Also the Fierz-Pauli mass can be arbitrarily large. However, to be physically meaningful it is limited by the Planck mass. In order to keep the problem under numeric control, we decided to choose more restrictive priors. At the same time we are interested in many different orders of magnitude. Therefore it is natural to work in a logarithmic scale. Explicitly, we use the uninformative priors

$$p(\bar{\alpha}) = \begin{cases} 1, & -100 < \log_{10}(\bar{\alpha}) < 2 \\ 0, & \text{else} \end{cases}, \quad p(\Omega_{\text{FP},0}) = \begin{cases} 1, & -2 < \log_{10}(\Omega_{\text{FP},0}) < 100 \\ 0, & \text{else} \end{cases}. \quad (6.4)$$

We should point out that the upper limit on $\bar{\alpha}$ implies that we do not expect the massive gravity limit of our models to be cosmologically viable [67–73]. The lower limit on Ω_{FP} is justified because we expect the value of the effective cosmological constant to be far away enough from zero for the

Higuchi bound to be relevant. The Fierz-Pauli mass cannot be arbitrary small. The upper bound does not correspond to the Planck scale but rather $m_{\text{FP}} \simeq 10^{19}$ eV, which is of the order of inflation scale. This limit ensures numerical stability of the evaluations as we checked by various examples.

6.2.2 Calculating the Hubble rate and likelihood

Now that we clarified where we want to compare the model to observations, let us explain how. Calculating the luminosity distance as theoretical prediction, requires integrating the Hubble rate over redshift z , see eq. (6.1). The redshift enters the Hubble rate via the matter energy density $\rho_m = \rho_m(z)$, cf. eq. (3.9), and via the scale factor ratio $y = y(z)$, cf. eq. (3.12). Since the bimetric models vary a lot in complexity, we use two different methods to construct $H(z)$.

For the simple β_1 - and $\beta_0\beta_1$ -models, Friedmann's equation is still handy. As described in the previous section we solved eq. (3.12) for y and picked the solution that describes the finite branch. Plugging the result into eq. (3.10a) yields the Hubble rate as a function of redshift z and we can perform the integration over z numerically in order to get the luminosity distance d_L . It is automatically guaranteed that the expansion history follows the finite branch.

For all the other models, this procedure turns out to be quite cumbersome and numerically slow. Instead, we employ the following strategy. We solve eq. (3.12) numerically for y at a given redshift z . This yields up to four solutions, out of which we pick the one that satisfies⁷ $0 < \bar{y}(z) < \bar{\alpha}$ to ensure that y evolves on the finite branch. With the resulting value for $y(z)$ we compute the value of the Hubble rate $H(z)$ at redshift z .

In contrast to the analysis of Ref. [16], we do not solve the differential equation that describes the evolution of y , cf. eq. (3.13). Instead, we compute the value for y and hence H for each redshift individually. Although this requires more computing time, there is no ambiguity in choosing initial conditions and y is guaranteed to evolve on the finite branch.

Having clarified how to compute the theoretical predictions, let us demonstrate how to calculate the likelihood. The absolute magnitude M of a supernova is degenerate with the value of the Hubble rate today, H_0 , as these appear as additive quantities⁸ in m . In order to remove the degeneracy, one can define a new variable which is the sum of both. This new variable however is not of interest for us in our cosmological data analysis and appears as a nuisance parameter. We wish to marginalize over the nuisance parameter. This can be done analytically by defining a marginalized χ^2 as

$$\tilde{\chi}^2(\theta) = \sum_i \frac{(5 \log_{10} D_L(\theta) - m(x_i))^2}{\sigma_i^2} - \frac{\left(\sum_i \frac{5 \log_{10} D_L(\theta) - m(x_i)}{\sigma_i^2} \right)^2}{\sum_i \sigma_i^{-2}}, \quad (6.5)$$

where D_L is the rescaled luminosity distance which can be computed from $E(z)$. In each step of the Markov chain we compute the quantity $\tilde{\chi}^2$. The likelihood is then given by

$$\mathcal{L}(\theta) = e^{-\frac{1}{2}\tilde{\chi}^2(\theta)}. \quad (6.6)$$

Having the minimum of the χ^2 -distribution for each model as a measure for the goodness of fit at hand, we would like to compare the different models. As a rough estimate for model comparison, we introduce the reduced χ^2 as

$$\tilde{\chi}_{\text{red}}^2 = \frac{\tilde{\chi}_{\text{min}}^2}{\text{d.o.f.}} \quad (6.7)$$

where the number of degrees of freedom is given by $\text{d.o.f.} = N - P$ in terms of the number of data points N and number of free parameters of the model P . In our case, we have $N = 580$ data points

⁷In the numerical analysis we also rescaled the scale factor ratio by α as $\bar{y} = \alpha y$ in analogy to $\bar{\alpha}$. Then Friedmann's equation and the quartic polynomial are completely independent of α .

⁸To see this, replace d_L by D_L which yields $m = \mathcal{M} + 5 \log_{10} D_L$, where $\mathcal{M} = M + 25 - 5 \log_{10} H_0$ implying that H_0 and M are degenerate parameters. In our analysis, we are not interested in the value of the astrophysical parameter M . Therefore, we marginalize over the parameter \mathcal{M} . Note that in this sense, supernovae do not provide constraints on H_0 .

Model	$\tilde{\chi}_{\min}^2$	$\tilde{\chi}_{\text{red}}^2$	$\Omega_{\text{m},0}$	$\Omega_{\Lambda,0}$	$\log_{10}(\bar{\alpha})$	$\log_{10}(\Omega_{\text{FP}})$	$\log_{10}(m_{\text{FP}} [\text{eV}])$
β_1	563.11	0.973	$0.38^{+0.02}_{-0.02}$	$0.79^{+0.01}_{-0.01}$	(-0.24)	$1.05^{+0.02}_{-0.02}$	$-31.24^{+0.01}_{-0.01}$
$\beta_0\beta_1$	562.22	0.973	$0.28^{+0.15}_{-0.02}$	$0.72^{+0.05}_{-0.02}$	-16^{+16}_{-84}	$-0.14^{+0.02}_{-0.02}$	$-31.84^{+0.01}_{-0.01}$
$\beta_1\beta_2$	562.23	0.973	$0.28^{+0.10}_{-0.02}$	$0.72^{+0.05}_{-0.02}$	-20^{+20}_{-30}	39^{+61}_{-39}	-12^{+30}_{-20}
$\beta_1\beta_3$	562.23	0.973	$0.30^{+0.08}_{-0.04}$	$0.70^{+0.07}_{-0.02}$	-1^{+1}_{-49}	2^{+98}_{-2}	-31^{+49}_{-1}
$\beta_1\beta_4$	562.23	0.973	$0.28^{+0.13}_{-0.02}$	$0.72^{+0.03}_{-0.08}$	-20^{+20}_{-30}	38^{+62}_{-38}	-13^{+31}_{-19}
$\beta_0\beta_1\beta_4$	562.19	0.974	$0.28^{+0.15}_{-0.02}$	$0.72^{+0.12}_{-0.05}$	-1^{+3}_{-99}	6^{+94}_{-6}	-29^{+47}_{-3}
$\beta_1\beta_2\beta_3$	562.23	0.974	$0.28^{+0.03}_{-0.02}$	$0.72^{+0.02}_{-0.02}$	-65^{+64}_{-35}	86^{+14}_{-87}	11^{+7}_{-43}
ΛCDM	562.25	0.971	$0.28^{+0.03}_{-0.02}$	$0.72^{+0.03}_{-0.02}$	-	-	-

Table 2: Summary of the best fit values for the one, two and three parameter models. To compute m_{FP} from $\Omega_{\text{FP},0}$ we use the local value of the Hubble rate, $H_0 = (73.24 \pm 1.74) \text{ km/s/Mpc} = (9.82 \pm 0.24) \text{ eV}$ [75]. The number of free parameters is given by the number of free β_n -parameters, while for the ΛCDM model there is one free parameter.

while the number of free parameters varies from model to model. Determining the correct number of effective free parameters of a model is not straightforward, in particular for nonlinear models or correlated parameters [74]. As we only want to give a rough estimate, we take P to be the number of free fitting parameters. With this value for P we tend to overestimate the value of $\tilde{\chi}_{\text{red}}^2$.

6.3 Results and discussion

In this section we discuss and summarize the results of the statistical analysis. The best-fit values for the physical parameters are summarized in table 2 for all models under consideration. Details on the chains can be found in appendix C.

Instead of discussing each model separately, let us first discuss what they have in common. The parameters $\Omega_{\text{m},0}$ and $\Omega_{\Lambda,0}$ are well-constrained by supernova data and their marginal posterior PDFs have a Gaussian shape. The marginal posterior PDFs for $\Omega_{\text{m},0}$ are depicted in fig. 3 for all models. The $\beta_0\beta_1$ -, $\beta_1\beta_2$ -, $\beta_1\beta_4$ -, and the 3-parameter models have roughly the same best-fit value for $\Omega_{\text{m},0}$ as the ΛCDM , while for the $\beta_1\beta_3$ -model the value of $\Omega_{\text{m},0}$ is slightly larger at the best-fit point. The β_1 -model has the largest value with $\Omega_{\text{m},0} = 0.38 \pm 0.02$. The reason can be understood from inspecting Friedmann's equation. The induced Dark Energy component contains a contribution that scales with redshift like non-relativistic matter, but with a negative sign [19]. This is most prominent in the β_1 -model (c.f. eq. (5.7)) as it does not have a GR-limit. Therefore, bimetric cosmology generically prefers a larger value of $\Omega_{\text{m},0}$ compared to ΛCDM with beneficial impact on the H_0 -tension [76].

Since the difference of $\Omega_{\text{m},0}$ to unity measures the amount of Dark Energy present in the universe today, bimetric theory needs less (or as much) Dark Energy compared to the ΛCDM model to explain the current accelerated expansion of the universe. Note that Dark Energy in bimetric theory, $\Omega_{\text{DE}} = 1 - \Omega_{\text{m}}$, is not constant, but evolves in time. Most importantly, within bimetric theory the universe can be filled with Dark Energy even in the absence of vacuum energy giving rise to self-acceleration. The models with $\beta_0 = 0$ are self-accelerating and in perfect agreement with observations. In this case, Dark Energy is composed only of interaction energy between the two metric tensors. Only asymptotically, i.e. in the infinite future, Dark Energy approaches a constant value, $\Omega_{\text{DE},0} \rightarrow \Omega_{\Lambda,0}$. The parameter $\Omega_{\Lambda,0}$ parametrizes the asymptotic effective cosmological constant and is a mixture of vacuum energy and interaction energy between the two metric tensors (unless the vacuum energy is set to zero, $\beta_0 = 0$). The effective cosmological constant is well-constrained by supernova data and the marginal posterior PDFs are Gaussian for all models. Here, we only report their best-fit value and 1σ intervals in table 2, without explicitly showing the marginalized posterior PDFs. Moreover, we can deduce that at current times Dark Energy is almost constant for all 2- and 3-parameter models because $\Omega_{\text{DE},0} = 1 - \Omega_{\text{m},0} \simeq \Omega_{\Lambda,0}$. Although we allowed for non-trivial behavior of the bimetric models, supernova data drives all models (except the β_1 -model) into a regime where Dark Energy behaves as a cosmological constant at current times.

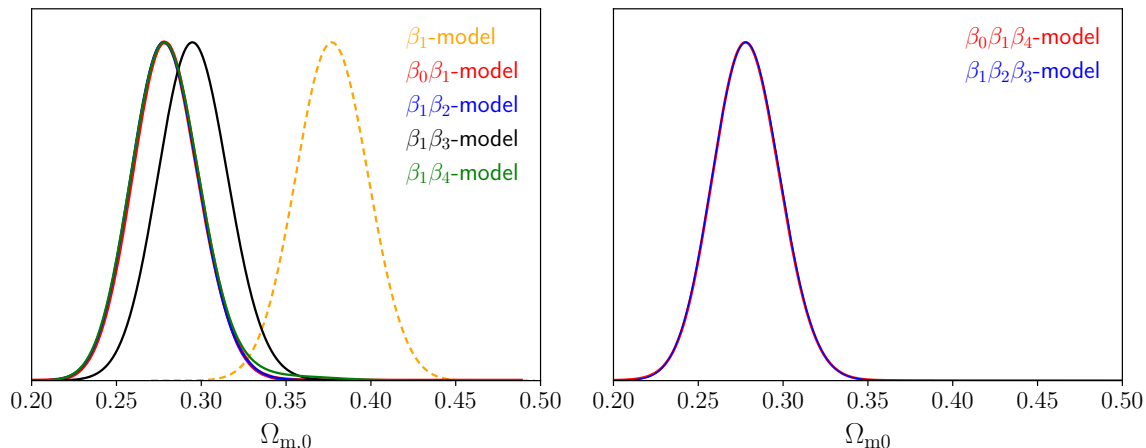
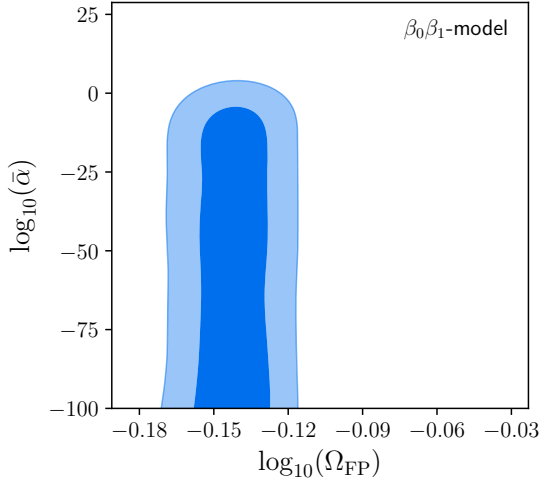


Figure 3: These figures show the marginalized posterior distribution for $\Omega_{m,0}$. The left panel shows the posterior for the one- and two-parameter models, while the right panel shows the posterior for the three-parameter models and the full model. The matter energy density parameter is the exact opponent to the dark energy density parameter $\Omega_{\text{DE},0} = 1 - \Omega_{m,0}$.

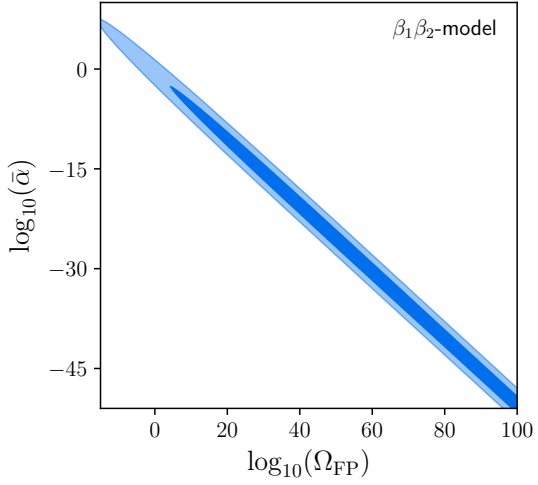
Let us move to the differences between the models. The β_1 -model has only one free parameter. Data constrains the Fierz-Pauli mass to be $m_{\text{FP}} = (5.71 \pm 0.18) \times 10^{-32}$ eV. The minimal bimetric model gives rise to self-acceleration consistent with data when the Fierz-Pauli mass is close to the Higuchi bound. Most notably, although the model does not possess a GR-limit ($\bar{\alpha}$ is fixed by the equations of motion), it fits the data almost as good as the Λ CDM model, with $\tilde{\chi}_{\text{min}}^2 \simeq 563.11$, while having the same number of free parameters.

Next let us move to the two parameter models. For the $\beta_0\beta_1$ -model, the spin-2 mass is well-constrained to $m_{\text{FP}} = (1.45 \pm 0.05) \times 10^{-32}$ eV, which lies close to the value of the cosmological constant. Hence, this model is driven into its GR-limit, cf. eq. (5.10). Consequently, the mixing angle must be sufficiently small, $\bar{\alpha} < 1$ at 1σ and data allows the mixing angle to be arbitrarily small, cf. 4a. The same happens in the other 2-parameter models as can be seen in figs. 4b to 4d. However, the correlation between $\bar{\alpha}$ and m_{FP} is different compared to the $\beta_0\beta_1$ -model. The spin-2 mass is not constrained by supernova data, but only forced to not be too small ($m_{\text{FP}} \gtrsim 10^{-32}$ eV at 1σ) for all three models. Their correlation is determined by the previously derived eqs. (5.16), (5.19) and (5.22) and summarized in fig. 1 with a value for the cosmological constant as reported in table 2. For the 2-parameter models, our priors (specifically the upper limit on the Fierz-Pauli mass and the lower limit on the mixing angle) cut through a region of the physical parameter space, where the models give a good fit to data. This, of course, is not surprising as we expect the GR-limit of these models to give a good fit to data, which is achieved by $\bar{\alpha} \ll 1$. In order to decide, whether data forces these models into their GR-limits, one needs to weaken the priors and include other observables. This is beyond the scope of the current work. Let us instead note that all the 2-parameter models fit the data as good as the Λ CDM model with $\tilde{\chi}_{\text{min}}^2 \simeq 562.2$ in all cases, while the latter remains statistically favored due to the smaller number of free parameters in the model. The models with $\beta_0 = 0$ do not inherit vacuum energy but give rise to self-acceleration solely due to the bimetric interaction energy.

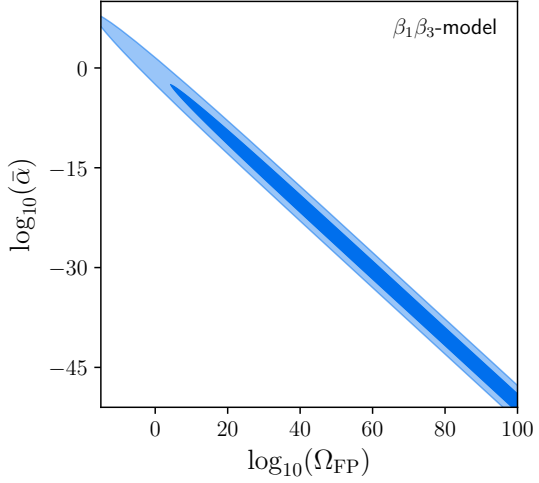
Let us move to the three parameter models, where the three physical parameters are independent of each other. As for the previous models, only the parameters $\Omega_{m,0}$ and $\Omega_{\Lambda,0}$ are well-constrained by data, while $\bar{\alpha}$ and m_{FP} remain mostly unconstrained. Although both three parameters are subject to completely different theoretical consistency requirements, data selects similar parameter regions for both of them as can be seen in fig. 5. For both models, the region where $\bar{\alpha}$ and m_{FP} are large are disfavored by data. For the $\beta_1\beta_2\beta_3$ -model this is obvious as this region does not satisfy our consistency requirements, cf. fig. 2. For the $\beta_0\beta_1\beta_4$ -model there is a different reason. From eq. (5.31)



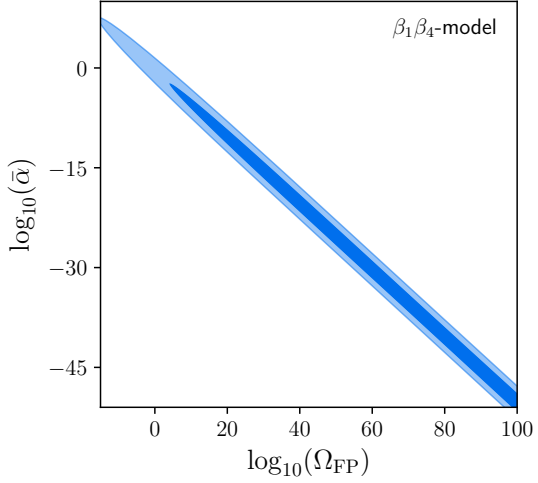
(a) 68% and 95% c.l. for the $\beta_0\beta_1$ -model



(b) 68% and 95% c.l. for the $\beta_1\beta_2$ -model



(c) 68% and 95% c.l. for the $\beta_1\beta_3$ -model



(d) 68% and 95% c.l. for the $\beta_1\beta_4$ -model

Figure 4: These plots show the regions of 68% (dark blue) and 95% (light blue) confidence level for all two parameter models with $\beta_1 \neq 0$. They represent the two-dimensional marginal posterior PDF in the $\bar{\alpha} - \Omega_{\text{FP}}$ -plane.

it follows that $\beta_0 < 0$ when

$$\bar{\alpha}^2 > \frac{\Lambda}{3m_{\text{FP}}^2 - \Lambda}. \quad (6.8)$$

Hence, data disfavors vacuum energy to be too negative. Since vacuum energy is constant in time (β_0 is time independent), but y evolves back in time towards zero, there is a point in the past where the Dark Energy density changes its sign and becomes negative because $\Omega_{\text{DE}} \rightarrow B_0$ as $y \rightarrow 0$. In principle, $\Omega_{\text{DE},0} < 0$ is allowed, which has to be counterbalanced by $\Omega_{\text{m},0} > 1$. Although theoretically consistent, this scenario is not favored by data. The point in time, where Ω_{DE} changes its sign, must be early enough for the model to be consistent with supernova data. Since supernovae only probe times up to a redshift of $z \lesssim 1.4$, we expect cosmic observables that probe earlier redshifts to put more stringent constraints on the parameter space of the $\beta_0\beta_1\beta_4$ -model.

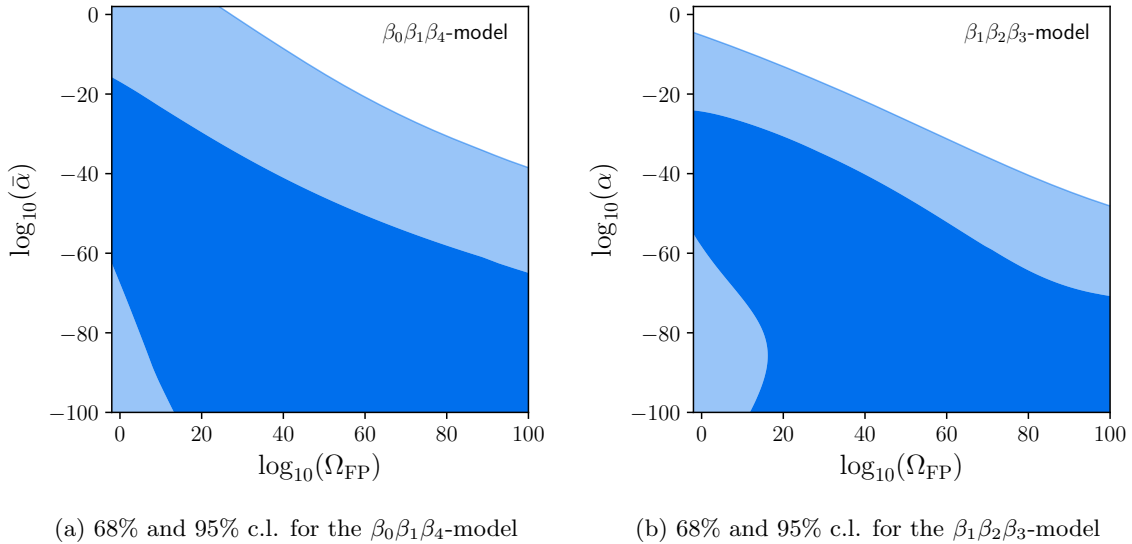


Figure 5: These plots show the 68% (dark blue) and 95% (light blue) confidence levels for the three parameter models under consideration. These represent the two-dimensional marginal posterior distribution in the $\bar{\alpha} - \Omega_{\text{FP}}$ -plane.

The region of the parameter space, where $\bar{\alpha}$ is small and the Fierz-Pauli mass is close the Higuchi bound seems to be slightly disfavored by data (2σ), cf. fig. 5. We believe that this is an artifact of numerical instability in that region. In order to see that, let us compare the value of $\tilde{\chi}^2$ for exemplary points in that region with the value $\tilde{\chi}_{\text{min}}^2$ for both models. Taking $\Omega_{\Lambda,0} = 0.72$, which is the likeliest value for both models, and exemplary values $\bar{\alpha} = 10^{-90}$ and $\Omega_{\text{FP}} = 3 \cdot 10^3$ yields $\tilde{\chi}^2 = 562.24$ for both models. For other exemplary parameter values we indeed find numerical instabilities in that region as we have checked explicitly. Hence we conclude that this region in fact is not less likely than the region enclosed by the 1σ contour

Let us finish the discussion of three-parameter models by noting that only the upper right region is disfavored by data, that is for large Fierz-Pauli mass m_{FP} and a not too small mixing angle $\bar{\alpha}$. The exact GR-limit for the model is excluded by the choice of priors (the upper limit on $\Omega_{\text{FP},0}$ and the lower limit on $\bar{\alpha}$), but we expect it to give a good fit to data as well. Whether data really forces the models into their GR-limits needs an extended scan of the parameter space which is beyond the scope of the current work. Besides that, a large portion of the physical parameter space is consistent with observations.

In our analysis, we use the local value of the Hubble rate, $H_0 = (73.24 \pm 1.74)$ km/s/Mpc, as reported in Ref. [75] in order to determine m_{FP} from Ω_{FP} . However, the true value of H_0 is still under debate since CMB data, for instance, implies a value of $H_0 = (67.36 \pm 0.54)$ km/s/Mpc [77]. With this value we obtain a spin-2 mass of $m_{\text{FP}} = (5.25 \pm 0.12)$ eV for the β_1 -model and $m_{\text{FP}} = (1.33 \pm 0.03)$ eV for the $\beta_0\beta_1$ -model, while the already large allowed mass ranges in the other models are not altered. Hence, taking the H_0 -tension seriously and using the global value of H_0 including its large errors would increase the allowed mass range. However, since in this paper we are dealing with low-redshift data only, we use the local value of H_0 instead of the global one.

7 Conclusions and outlook

We proposed a method to relate the parameters of bimetric theory to its physical parameters. The physical parameters are per definition entities of vacuum solutions and since bimetric theory has several (up to four) vacua the relation between the theory and physical parameters is a priori not unique. However, imposing theoretical consistency requirements on the vacua and on the expansion

history of the universe, singles out a unique vacuum solution as the true vacuum. This results in a unique relation between the theory and physical parameters and allows to build up a dictionary between these parametrizations.

We worked out the dictionary for all (sub-)models of bimetric theory where the identification of the unique vacuum works analytically. These are the models with one, two or three free interaction parameters β_n .

The physical parametrization has several advantages. The consistency requirements summarized in this paper for each model and the direct physical interpretation provides intuition for the numerical values of the parameters. This, e.g., vastly simplifies choosing priors for data analysis. In addition, non-linear solutions of bimetric theory that are sensitive to the individual theory parameters can directly be compared to linear solutions that are only sensitive to the physical parameters.

In order to demonstrate these features of the physical parametrization we applied our method to FLRW solutions. As a first step towards combining various tests of gravity into a single framework we performed a statistical analysis using supernova data to constrain the physical parameter space of bimetric theory.

All the models that we considered show quite similar behavior with only few exception. We find that energy density of non-relativistic matter today is roughly the same as in GR for all models, varying from $\Omega_{m,0} = 0.28$ up to $\Omega_{m,0} = 0.38$ for different models. The gap to the critical energy density is filled by Dark Energy, that in bimetric theory is dynamical and either solely due to interaction energy between the massive and the massless spin-2 field (models where $\beta_0 = 0$) or due to a combination of vacuum and interaction energy. Dark Energy approaches a constant value in the asymptotic future (which corresponds to the cosmological constant of the asymptotic de Sitter spacetime) that we denote by $\Omega_{\Lambda,0}$. Although we allowed for nontrivial deviations from GR at late times, data favors all the models to act like Λ CDM at late times. That is the dynamical Dark Energy component is almost constant at late times, $\Omega_{DE,0} = 1 - \Omega_{m,0} \approx \Omega_{\Lambda,0}$. The only exception here is the β_1 -model that does not have a GR-limit and is self-accelerating.

Let us summarize the constraints on the mass, m_{FP} , and the coupling strength to ordinary matter, $\bar{\alpha}$, of the massive spin-2 field. These constraints are highly model dependent. For the minimal model where only β_1 is a free parameter the coupling strength is fixed to $\bar{\alpha} = 1/\sqrt{3}$. Data then favors a spin-2 mass of $m_{\text{FP}} = (5.71 \pm 0.18) \times 10^{-32}$ eV, which lies close to the Higuchi bound. For the $\beta_0\beta_1$ -model the spin-2 mass is constrained to $m_{\text{FP}} = (1.45 \pm 0.05) \times 10^{-32}$ eV while the mixing angle is only constrained to not be too large ($\bar{\alpha} \lesssim 1$ at 1σ). The other two parameter models show very similar behavior. The physical parameters are degenerate and mostly unconstrained. The coupling strength is constrained to be $\bar{\alpha} < 1$ and the mass $m_{\text{FP}} > 10^{-32}$ eV at 1σ . For large masses, the coupling strength and the mass are fixed by the best-fit value of the cosmological constant as $\bar{\alpha}^2 m_{\text{FP}}^2 = \kappa\Lambda$, where $\kappa = \mathcal{O}(1)$ is a model dependent number⁹. Note that we use the local Hubble value to determine m_{FP} , while the allowed mass range would increase when using the global value. Moving to the three parameter models, the strict relation between $\bar{\alpha}$ and m_{FP} is relaxed and all physical parameters are really independent. The observational constraints on $\bar{\alpha}$ and m_{FP} are weak, only the region where $\bar{\alpha}^2 m_{\text{FP}}^2 \gg \Lambda$ is disfavored. Bimetric theory has self-accelerating solutions even when the spin-2 mass is large that are compatible with supernova data. On the other hand, the statistical analysis performed in this paper favors the Λ CDM-model either due to the smaller number of free parameters or due to a slightly larger likelihood.

Our results generalize the existing cosmological constraints from background observables on bimetric theory to the entire physical parameter space. While Refs. [14, 16] do not distinguish between the finite and infinite branch solution to the equations of motion, Refs. [15, 16, 27] compute constraints on the interaction parameters β_n . In Refs. [15, 16, 28] either the rescaled parametrization with $\alpha = 1$ is used or $B_n \sim \mathcal{O}(1)$ is assumed implying that their results apply only to a small region of the parameter space. As a consequence, Refs. [14–16, 28] test the region where the Fierz-Pauli mass is comparable to the Hubble rate today. This parameter region is the relevant one for addressing the H_0 -tension [76]. Due to the different parametrizations, it is non-trivial to relate our constraints on

⁹To be precise, $\kappa = 6$ for the $\beta_1\beta_2$, $\kappa = 4$ for the $\beta_1\beta_3$, and $\kappa = 3$ for the $\beta_1\beta_4$ -model. This follows from expanding the consistent vacuum solutions eqs. (5.16), (5.19) and (5.22) for $m_{\text{FP}}^2 \gg \Lambda$.

the bimetric parameters to these earlier works. Nonetheless, we can compare the constraints on $\Omega_{m,0}$ and find that they agree for all models that we consider.

As argued in Ref. [76, 78], the Vainshtein mechanism [5, 22] is expected to be active also in cosmology. It implies that deviations from GR are suppressed for energies larger than the spin-2 mass, i.e. for $H \gg m_{\text{FP}}$, while deviations are possibly testable at later times. This however depends on $\bar{\alpha}$ since a small coupling to standard matter suppresses deviations from GR at all redshifts. That means that supernova data could in principle test this effect in the parameter region where $\bar{\alpha} \gtrsim \mathcal{O}(1)$ and where $m_{\text{FP}} \lesssim 2 \times 10^{-32}$ eV, to give a rough estimate. This energy scale corresponds to the redshift $z \simeq 1.4$, up to which supernova data exists. Our analysis shows that most of this parameter region is excluded by supernova data (to be precise, $\alpha > 1$ is excluded at 95% c.l.). Hence, cosmological observables that probe higher redshifts are necessary to test the cosmological Vainshtein mechanism.

The next step on the level of background cosmology is to include more cosmological observables to find stronger constraints on the physical parameter space. The constraints from background cosmology can then be combined with constraints from other observables. While for galaxy cluster scales to galactic scales first results were obtained [21, 79–81] they still need to be put into a single framework. Also a consistent inclusion of the Vainshtein screening mechanism is (partly) lacking. On smaller scales, say solar system and below, some constraints on the parameter space were derived in Ref. [79]. A comprehensive analysis including the Vainshtein screening mechanism still needs to be done. Local and laboratory tests of gravity are reviewed in, e.g., Refs. [23, 82–85].

The second large class of constraints comes from the perturbative level. Although the linear perturbations on the finite branch are necessarily plagued by a gradient instabilities [17, 26, 48, 86, 87], we can always go to a limit of bimetric theory such that the instabilities occur only above a certain cutoff scale [42]. This scale is set by the Fierz-Pauli mass [76]. In this limit bimetric theory behaves like GR and all possibly testable deviations from the Λ CDM predictions are suppressed. However, a gradient instability only signals a breakdown of perturbation theory. There is good evidence that the instabilities are cured either due to the onset of the local Vainshtein mechanism [88] or due to the aforementioned time-dependent analogue of the Vainshtein mechanism [76, 78]. Indeed, the authors of Ref. [89] analyzed a fully non-linear but simplified setup and did not find any instability at all. These are promising hints that the FLRW solutions to bimetric theory are well-defined. A new treatment of cosmological perturbations needs to be established in order to deal with constraints coming from the perturbative level within bimetric theory.

Summarizing, in this paper we took a step towards combining various observable constraints. There is a large portion of the physical parameter space that is consistent with supernova data. If the massive spin-2 field should also account for the observed Dark Matter abundance in the Universe, it must be heavy (depending on the production mechanism, MeV to TeV) [19, 20]. Remarkably, our analysis shows that a heavy spin-2 field is in perfect agreement with supernova data. The reason is that the Fierz-Pauli mass and the effective cosmological constant are independent of each other and can be of a completely different energy scale. This opens up the possibility that bimetric theory can account for Dark Energy and simultaneously provides Dark Matter. While this seems to be excluded due to perturbativity bounds, answering this question requires further study.

Acknowledgements

M.L. acknowledges Julio A. Méndez-Zavaleta, who joined the project at an early stage. M.L. further thanks Georgia Pollina, Nico Hamaus and Martin Kerscher for their help regarding the data analysis and Angelo Caravano for useful comments on the manuscript. The authors also thank the anonymous referee for useful comments. This work is supported by a grant from the Max Planck Society.

A Example: Tuning of the interaction parameters

In this appendix we discuss the constant and singular roots for a concrete example, the $\beta_1\beta_2$ -model. Setting $\beta_0 = \beta_3 = \beta_4 = 0$ yields the background equation

$$3\alpha^2\beta_2c^3 + 3\alpha^2\beta_1c^2 - 3\beta_2c - \beta_1 = 0. \quad (\text{A.1})$$

This equation represents a polynomial in c of degree 3 such that it has up to three real-valued roots. Instead of presenting the full solutions, let us jump to the limit $\alpha \ll 1$ immediately. We find the constant root

$$c_c = -\frac{\beta_1}{3\beta_2} + \mathcal{O}(\alpha^2). \quad (\text{A.2})$$

In order for the root to be positive valued, we need $\beta_2 < 0$. Plugging this root into the expressions for the Fierz-Pauli mass and the cosmological constant, we arrive at

$$m_{\text{FP}}^2 = -\frac{\beta_2}{\alpha^2} + \mathcal{O}(1), \quad (\text{A.3a})$$

$$\Lambda = -\frac{2}{3} \frac{\beta_1^2}{\beta_2} + \mathcal{O}(\alpha^2). \quad (\text{A.3b})$$

For $\beta_2 < 0$, both quantities are positive. This explicitly demonstrates that $\alpha \ll 1$ implies $m_{\text{FP}}^2 \gg \Lambda$ without further tuning on a constant root.

Let us move to the singular roots, that in the limit $\alpha \ll 1$ read

$$c_{s\pm} = \pm \frac{1}{\alpha} - \frac{\beta_1}{3\beta_2} + \mathcal{O}(\alpha^2), \quad (\text{A.4})$$

of which $c_{s+} > 0$. On this singular root, the Fierz-Pauli mass and cosmological constant are given by

$$m_{\text{FP}}^2 = \frac{4\beta_2}{\alpha^2} + \mathcal{O}(1), \quad (\text{A.5a})$$

$$\Lambda = \frac{3\beta_2}{\alpha^2} + \mathcal{O}(1). \quad (\text{A.5b})$$

Both quantities are positive valued only for $\beta_2 > 0$ in contrast to the constant root. Note that $\alpha \ll 1$ does not imply that the Fierz-Pauli mass is much larger than the cosmological constant. Instead, they are of the same order of magnitude, but still satisfy the Higuchi bound. In order to achieve a hierarchy between both quantities requires tuning one of the β_n parameters, e.g. $\beta_2 = \beta_2(\alpha, \beta_1)$.

B Dictionary for the three parameter models

In this appendix, we identify the consistent vacua and complete the dictionary between the theory and physical parameters for the remaining three parameter models, but without comparing these models to data.

B.0.1 $\beta_0\beta_1\beta_2$ model

For $\beta_3 = \beta_4 = 0$, eq. (2.14) has the following roots

$$\bar{\alpha}_{\pm} = \pm \sqrt{\frac{m_{\text{FP}} - \Lambda + \bar{\beta}_2}{\Lambda - \bar{\beta}_2}}, \quad (\text{B.1})$$

where $\bar{\beta}_2 = \alpha^{-2}\beta_2$. The root $\bar{\alpha}_-$ is always non-positive and we dismiss it. The root $\bar{\alpha}_+$ is real-valued in the parameter range $\Lambda - m_{\text{FP}}^2 < \bar{\beta}_2 < \Lambda$. Solving this relation for β_2 , we can express all interaction parameters in terms of physical parameters as

$$\beta_0 = \frac{\bar{\alpha}^2(-6m_{\text{FP}}^2 + 4\Lambda) + (1 + 3\bar{\alpha}^4)\Lambda}{1 + \bar{\alpha}^2} \quad (\text{B.2a})$$

$$\alpha^{-1}\beta_1 = \bar{\alpha} \left(\frac{3m_{\text{FP}}^2}{1 + \bar{\alpha}^2} - 2\Lambda \right) \quad (\text{B.2b})$$

$$\alpha^{-2}\beta_2 = \frac{(1 + \bar{\alpha}^2)\Lambda - m_{\text{FP}}^2}{1 + \bar{\alpha}^2} \quad (\text{B.2c})$$

The vacuum point $\bar{\alpha}_+$ is well-defined in the whole parameter space, when the Higuchi bound is satisfied. However, requiring $\beta_1 > 0$ imposes a bound on the parameter space,

$$3m_{\text{FP}}^2 > 2(1 + \bar{\alpha}^2)\Lambda. \quad (\text{B.3})$$

The left panel of fig. 6 shows the theoretically consistent parameter space of the $\beta_0\beta_1\beta_2$ -model. In the red-shaded region eq. (B.3) is violated and hence unphysical. Translating the bound on β_2 yields the same condition in the physical parameters.

B.0.2 $\beta_0\beta_1\beta_3$ model

For $\beta_2 = \beta_4 = 0$, the polynomial eq. (2.14) has four roots, of which the possibly positive ones read.

$$\bar{\alpha}_{\pm} = \sqrt{\frac{4m_{\text{FP}}^2 - 2\Lambda + \beta_0 \pm \sqrt{(4m_{\text{FP}}^2 + \beta_0)^2 - 16m_{\text{FP}}^2\Lambda}}{2\Lambda}}. \quad (\text{B.4})$$

The other two roots are $-\bar{\alpha}_{\pm}$ and hence non-positive in the entire parameter space. Both roots are real-valued only if $\beta_0 > 4m_{\text{FP}}(\sqrt{\Lambda} - m_{\text{FP}})$. In this parameter range we find that $\bar{\alpha}_+$ can never be smaller than $\bar{\alpha}_-$. This identifies $\bar{\alpha}_-$ as the unique vacuum. It is real-valued in the parameter range $4m_{\text{FP}}(\sqrt{\Lambda} - m_{\text{FP}}) < \beta_0 < \Lambda$. Solving the expression for $\bar{\alpha}_-$ for β_0 yields

$$\beta_0 = \frac{\bar{\alpha}^2(-4m_{\text{FP}}^2 + 2\Lambda) + (1 + \bar{\alpha}^2)\Lambda}{1 + \bar{\alpha}^2} \quad (\text{B.5a})$$

$$\alpha^{-1}\beta_1 = -\bar{\alpha} \frac{-3m_{\text{FP}}^2 + (1 + \bar{\alpha}^2)\Lambda}{2(1 + \bar{\alpha}^2)} \quad (\text{B.5b})$$

$$\alpha^{-3}\beta_3 = \frac{-m_{\text{FP}}^2 + (1 + \bar{\alpha}^2)\Lambda}{2\bar{\alpha}(1 + \bar{\alpha}^2)} \quad (\text{B.5c})$$

where we already simplified the expressions using the bound eq. (B.8). The constraints on β_0 translate as

$$4m_{\text{FP}}^2 > (1 + \bar{\alpha}^2)\Lambda. \quad (\text{B.6})$$

Outside this parameter range, the vacuum $\bar{\alpha}_-$ is not well-defined. This bound is weaker than the other bounds and represented by the blue dashed line in fig. 6. The requirement $\beta_1 > 0$ is satisfied in the parameter region where

$$3m_{\text{FP}}^2 > (1 + \bar{\alpha}^2)\Lambda, \quad (\text{B.7})$$

which is indicated by the red-shaded region in fig. 6.

Moving to cosmology, we expand the expression for $\rho_{\text{m}}(y)$ around $y = \bar{\alpha}/\alpha$ and find that it only vanishes if

$$4m_{\text{FP}}^2 > (1 + \bar{\alpha}^2)^2\Lambda \quad (\text{B.8})$$

is satisfied. This bound is represented by the blue-shaded region. In this parameter range, β_1 is guaranteed to be positive and represents the most stringent bound on the parameter space. Only if these bounds are satisfied, the $\beta_0\beta_1\beta_3$ model can give rise to a viable expansion history. The bounds are collected in the right panel of fig. 6.

B.0.3 $\beta_1\beta_2\beta_4$ model

Setting $\beta_0 = \beta_3 = 0$, eq. (2.14) has four roots, of which the two possibly positive ones are given by

$$\bar{\alpha}_{\pm} = \sqrt{\frac{3m_{\text{FP}}^2 - \Lambda + 3\bar{\beta}_2 \pm \sqrt{(3m_{\text{FP}}^2 - \Lambda - 3\bar{\beta}_2)^2 - 12\bar{\beta}_2\Lambda}}{6\bar{\beta}_2}}, \quad (\text{B.9})$$

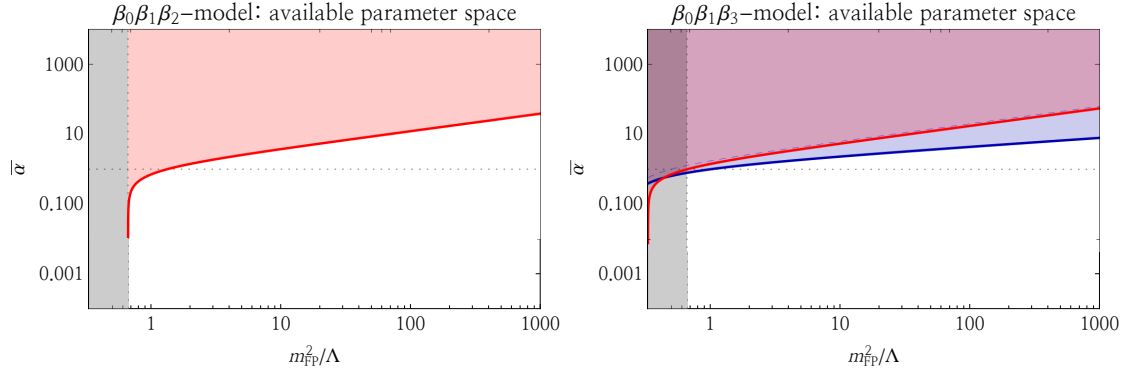


Figure 6: Left: The theoretically consistent parameter space for the $\beta_0\beta_1\beta_2$ model. In the red-shaded region the condition $\beta_1 > 0$ is violated. Right: The theoretically consistent parameter space of the $\beta_0\beta_1\beta_3$ model. The blue-shaded region is excluded because the asymptotic future is not well-defined. In the red-shaded region the bound $\beta_1 > 0$ is violated. The blue dashed line indicates the bound eq. (B.6). In both plots, the gray-shaded region indicates violation of the Higuchi bound.

where $\bar{\beta}_2 = \alpha^{-2}\beta_2$. The other two roots are given by $-\bar{\alpha}_\pm$ and we neglect them. A necessary condition for both roots to be real-valued is

$$3\bar{\beta}_2 < 3m_{\text{FP}}^2 - 2\sqrt{3}m_{\text{FP}}\sqrt{\Lambda} + \Lambda. \quad (\text{B.10})$$

Furthermore, the root $\bar{\alpha}_+$ is real valued only if additionally $\beta_2 > 0$. In this parameter range $\bar{\alpha}_- < \bar{\alpha}_+$ always. This identifies $\bar{\alpha}_-$ as the unique consistent vacuum of the $\beta_1\beta_2\beta_4$ model in the viable parameter range defined by eq. (B.10).

Solving the expression for $\bar{\alpha}_-$ for the remaining interaction parameter β_2 yields the following dictionary

$$\alpha^{-1}\beta_1 = \frac{\bar{\alpha}^2(-3m_{\text{FP}}^2 + 2\Lambda) + 2\Lambda}{2\bar{\alpha}(1 + \bar{\alpha}^2)}, \quad (\text{B.11a})$$

$$\alpha^{-2}\beta_2 = \frac{\bar{\alpha}^2(3m_{\text{FP}}^2 - \Lambda) - \Lambda}{3\bar{\alpha}^2(1 + \bar{\alpha}^2)}, \quad (\text{B.11b})$$

$$\alpha^{-4}\beta_4 = \frac{\bar{\alpha}^2(-6m_{\text{FP}}^2 + 4\Lambda) + (1 + 3\bar{\alpha}^4)\Lambda}{3\bar{\alpha}^4(1 + \bar{\alpha}^2)}, \quad (\text{B.11c})$$

where we already used the bound (B.13) to simplify expressions. The consistency requirement $\beta_1 > 0$ is satisfied if

$$3\bar{\alpha}^2 m_{\text{FP}}^2 < 2(1 + \bar{\alpha}^2)\Lambda. \quad (\text{B.12})$$

In the red-shaded region in the left panel of fig. 6 this bound is violated.

Moving to cosmology, the finite branch is well-defined if

$$3\bar{\alpha}^4 m_{\text{FP}}^2 < (1 + \bar{\alpha}^2)^2 \Lambda \quad (\text{B.13})$$

is satisfied. The blue-shaded region in the left panel of fig. 6 indicates, where this bound is violated.

B.0.4 $\beta_1\beta_3\beta_4$ model

For $\beta_0 = \beta_2 = 0$ the background eq. (2.14) has three roots, only one of which is possibly real-valued,

$$\bar{\alpha} = \frac{1}{6\beta_1} \left(-m_{\text{FP}}^2 + \Lambda + \frac{-12\bar{\beta}_1^2 + (m_{\text{FP}}^2 - \Lambda)^2}{\mathcal{B}^{1/3}} + \mathcal{B}^{1/3} \right), \quad (\text{B.14})$$

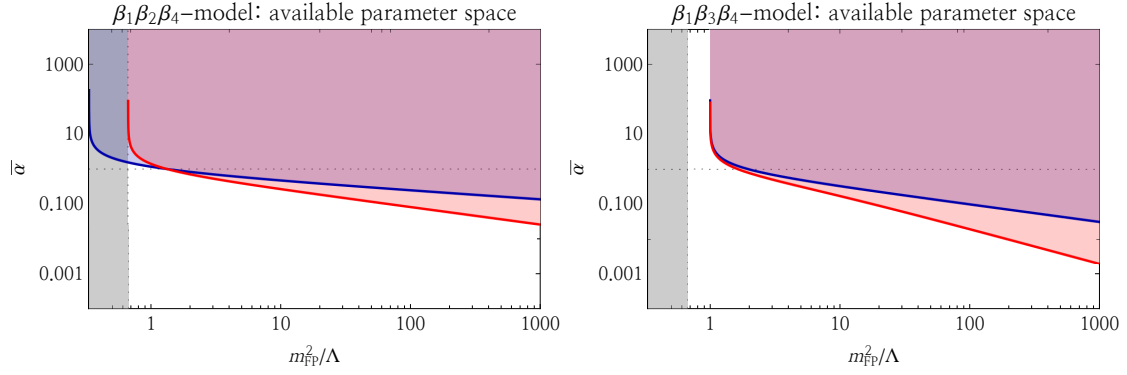


Figure 7: Left: The theoretically consistent parameter space for the $\beta_1\beta_2\beta_4$ model. In the blue-shaded region the finite branch is not well-defined, while in the red-shaded region $\beta_1 > 0$ is violated. Right: The theoretically consistent parameter space for the $\beta_1\beta_3\beta_4$ model. In the red-shaded region the bound $\beta_1 > 0$ is violated, while in the blue-shaded region the vacuum point is not well-defined. In both plots, the gray-shaded region indicates violation of the Higuchi bound.

where

$$\mathcal{B} = -(m_{\text{FP}}^2 - \Lambda)^3 + 18\bar{\beta}_1^2(m_{\text{FP}}^2 + 2\Lambda) + 6\bar{\beta}_1\sqrt{48\bar{\beta}_1^4 - 3(m_{\text{FP}}^2 - \Lambda)^3\Lambda - 3\bar{\beta}_1^2(m_{\text{FP}}^4 - 20m_{\text{FP}}^2\Lambda - 8\Lambda^2)}. \quad (\text{B.15})$$

By means of analytical and numerical methods, we find that the root is real-valued and positive if

$$\alpha^{-1}\beta_1 > \frac{\sqrt{m_{\text{FP}}^4 - 8\Lambda^2 + m_{\text{FP}}(m_{\text{FP}}^2 + 8\Lambda)^{3/2}}}{4\sqrt{2}}, \quad (\text{B.16})$$

which represents a nontrivial bound only if $m_{\text{FP}}^2 > \Lambda$. Solving the expression for $\bar{\alpha}$ for β_1 and plugging the result into the expressions for the other interaction parameters yields the following map:

$$\alpha^{-1}\beta_1 = \frac{-\bar{\alpha}^2 m_{\text{FP}}^2 + (1 + \bar{\alpha}^2)\Lambda}{2\bar{\alpha}(1 + \bar{\alpha}^2)}, \quad (\text{B.17a})$$

$$\alpha^{-3}\beta_3 = \frac{\bar{\alpha}^2(3m_{\text{FP}}^2 - \Lambda) - \Lambda}{2\bar{\alpha}^3(1 + \bar{\alpha}^2)}, \quad (\text{B.17b})$$

$$\alpha^{-4}\beta_4 = \frac{-4\bar{\alpha}^2 m_{\text{FP}}^2 + (1 + \bar{\alpha}^2)^2\Lambda}{\bar{\alpha}^4(1 + \bar{\alpha}^2)}, \quad (\text{B.17c})$$

The consistency bound (B.16) on the parameters translates into

$$4(1 + \bar{\alpha}^2)^3\Lambda^2 > \bar{\alpha}^2(2(1 + \bar{\alpha}^2)\Lambda + m_{\text{FP}}^2)^2. \quad (\text{B.18})$$

The blue-shaded region in the right panel of fig. 7 indicates, where this bound is violated. The bound $\beta_1 > 0$ is satisfied in the parameter region where

$$\bar{\alpha}^2 m_{\text{FP}}^2 < (1 + \bar{\alpha}^2)\Lambda. \quad (\text{B.19})$$

The red-shaded region in the right panel of fig. 6 represents the region of the parameter space, where $\beta_1 > 0$ is violated. Note that for this submodel, the small strip between the Higuchi bound and $m_{\text{FP}}^2 = \Lambda$ is not excluded by out consistency requirements.

C Details of the scan

In order to be explicit, in this appendix we report how we set up our MCMCs and comment on their convergence. For each model, we set up three independent MCMCs with different starting points. The free scanning parameters vary from model to model and are summarized in table 3.

Model	Scanning parameters	$\mathcal{R} - 1$
β_1	$\Omega_{m,0}$	0.003
$\beta_0\beta_1$	$\log_{10}(\bar{\alpha}), \log_{10}(\Omega_{\text{FP}})$	0.001
$\beta_1\beta_2$	$\log_{10}(\Omega_{\text{FP}}), \Omega_{\Lambda}$	0.008
$\beta_1\beta_3$	$\log_{10}(\Omega_{\text{FP}}), \Omega_{\Lambda}$	0.004
$\beta_1\beta_4$	$\log_{10}(\Omega_{\text{FP}}), \Omega_{\Lambda}$	0.002
$\beta_0\beta_1\beta_4$	$\log_{10}(\bar{\alpha}), \log_{10}(\Omega_{\text{FP}}), \Omega_{\Lambda}$	0.01
$\beta_1\beta_2\beta_3$	$\log_{10}(\bar{\alpha}), \log_{10}(\Omega_{\text{FP}}), \Omega_{\Lambda}$	0.008

Table 3: For different models we used a different set of free scanning parameters over which the MCMC runs. For the full model we choose to use $\sin^{-1}(B_{1,4})$ because it allows to scan many orders of magnitude for both positive and negative values. In addition, we report the value of the Gelman-Rubin factor \mathcal{R} . For sufficient convergence, the factor should be $\mathcal{R} - 1 \lesssim 0.01$.

For the β_1 -model, the MCMCs run over $\Omega_{m,0}$ with a variance of 0.01 and the three starting point $\{0.1, 0.5, 0.8\}$. We stop the chain after 15000 steps and remove 100 steps as burn-in. This yields a Gelman-Rubin factor of $\mathcal{R} - 1 \simeq 0.003$. Since we have only one parameter this already provides enough statistics and the chains have nicely converged.

For the $\beta_0\beta_1$ -model, the MCMCs run over $\log \bar{\alpha}$ with starting points $\{1, -10, -50\}$ and over $\log \Omega_{\text{FP}}$ with starting points $\{1, 1, 1\}$. Stopping the chain after 150000 steps and removing 6500 steps as burn-in yields a Gelman-Rubin factor of $\mathcal{R} - 1 \simeq 0.001$.

For the remaining two parameter models, we use the same scanning parameters and starting points. $\log_{10} \Omega_{\text{FP}}$ starts at $\{1, 50, 80\}$ and Ω_{Λ} at $\{0.5, 0.1, 0.8\}$. In each case we remove 500 steps as burn-in. The Gelman-Rubin factors for the three Markov chain for each model is $\mathcal{R} - 1 \approx 0.008$ for $\beta_1\beta_2$, $\mathcal{R} - 1 \simeq 0.004$ for $\beta_1\beta_3$, and $\mathcal{R} - 1 \approx 0.002$ for $\beta_1\beta_4$ signaling sufficient convergence.

Moving two the three parameter models, we only considered the two extreme cases and used the same scanning parameters. The parameter $\log_{10} \bar{\alpha}$ starts at $\{-1, -70, -70\}$, the parameter $\log_{10} \Omega_{\text{FP}}$ at $\{1, 10, 70\}$, and Ω_{Λ} starts at $\{0.7, 0.7, 0.7\}$ for both models. We remove 500 steps as burn-in. The Gelman-Rubin factor is $\mathcal{R} - 1 \approx 0.01$ for the $\beta_0\beta_1\beta_4$ -model and $\mathcal{R} - 1 \approx 0.008$ for the $\beta_1\beta_2\beta_3$ -model.

Summarizing, all our Markov chains suggest sufficient convergence and provide enough statistics for parameter inference.

References

- [1] W. Pauli and M. Fierz. On Relativistic Field Equations of Particles With Arbitrary Spin in an Electromagnetic Field. *Helv. Phys. Acta*, 12:297–300, 1939.
- [2] M. Fierz and W. Pauli. On relativistic wave equations for particles of arbitrary spin in an electromagnetic field. *Proc.Roy.Soc.Lond.*, A173:211–232, 1939.
- [3] H. van Dam and M.J.G. Veltman. Massive and massless Yang-Mills and gravitational fields. *Nucl.Phys.*, B22:397–411, 1970.
- [4] V.I. Zakharov. Linearized gravitation theory and the graviton mass. *JETP Lett.*, 12:312, 1970.
- [5] A.I. Vainshtein. To the problem of nonvanishing gravitation mass. *Phys.Lett.*, B39:393–394, 1972.
- [6] D.G. Boulware and Stanley Deser. Can gravitation have a finite range? *Phys.Rev.*, D6:3368–3382, 1972.
- [7] Claudia de Rham and Gregory Gabadadze. Generalization of the Fierz-Pauli Action. *Phys.Rev.*, D82:044020, 2010.
- [8] Claudia de Rham, Gregory Gabadadze, and Andrew J. Tolley. Resummation of Massive Gravity. *Phys.Rev.Lett.*, 106:231101, 2011.
- [9] S.F. Hassan and Rachel A. Rosen. On Non-Linear Actions for Massive Gravity. *JHEP*, 1107:009, 2011.
- [10] S.F. Hassan and Rachel A. Rosen. Resolving the Ghost Problem in non-Linear Massive Gravity. *Phys.Rev.Lett.*, 108:041101, 2012.

- [11] S.F. Hassan and Rachel A. Rosen. Bimetric Gravity from Ghost-free Massive Gravity. *JHEP*, 1202:126, 2012.
- [12] S.F. Hassan and Rachel A. Rosen. Confirmation of the Secondary Constraint and Absence of Ghost in Massive Gravity and Bimetric Gravity. *JHEP*, 1204:123, 2012.
- [13] Angnis Schmidt-May and Mikael von Strauss. Recent developments in bimetric theory. *J. Phys.*, A49(18):183001, 2016.
- [14] Mikael von Strauss, Angnis Schmidt-May, Jonas Enander, Edvard Mörtsell, and S.F. Hassan. Cosmological Solutions in Bimetric Gravity and their Observational Tests. *JCAP*, 1203:042, 2012.
- [15] Frank Könnig, Aashay Patil, and Luca Amendola. Viable cosmological solutions in massive bimetric gravity. *JCAP*, 1403:029, 2014.
- [16] Yashar Akrami, Tomi S. Koivisto, and Marit Sandstad. Accelerated expansion from ghost-free bigravity: a statistical analysis with improved generality. *JHEP*, 1303:099, 2013.
- [17] Antonio De Felice, A. Emir Gümrükçüoğlu, Shinji Mukohyama, Norihiro Tanahashi, and Takahiro Tanaka. Viable cosmology in bimetric theory. *JCAP*, 1406:037, 2014.
- [18] Eugeny Babichev, Luca Marzola, Martti Raidal, Angnis Schmidt-May, Federico Urban, Hardi Veermae, and Mikael von Strauss. Bigravitational origin of dark matter. *Phys. Rev.*, D94(8):084055, 2016.
- [19] Eugeny Babichev, Luca Marzola, Martti Raidal, Angnis Schmidt-May, Federico Urban, Hardi Veermae, and Mikael von Strauss. Heavy spin-2 Dark Matter. *JCAP*, 1609(09):016, 2016.
- [20] Xiaoyong Chu and Camilo Garcia-Cely. Self-interacting Spin-2 Dark Matter. *Phys. Rev.*, D96(10):103519, 2017.
- [21] Moritz Platscher, Juri Smirnov, Sven Meyer, and Matthias Bartelmann. Long Range Effects in Gravity Theories with Vainshtein Screening. *JCAP*, 1812(12):009, 2018.
- [22] Eugeny Babichev and Marco Crisostomi. Restoring general relativity in massive bigravity theory. *Phys. Rev.*, D88(8):084002, 2013.
- [23] Clifford M. Will. The Confrontation between General Relativity and Experiment. *Living Rev. Rel.*, 17:4, 2014.
- [24] Marvin Lüben, Edvard Mörtsell, and Angnis Schmidt-May. Bimetric cosmology is compatible with local tests of gravity. *Class. Quant. Grav.*, 37(4):047001, 2020.
- [25] Adam R. Solomon, Yashar Akrami, and Tomi S. Koivisto. Linear growth of structure in massive bigravity. *JCAP*, 1410:066, 2014.
- [26] Frank Könnig, Yashar Akrami, Luca Amendola, Mariele Motta, and Adam R. Solomon. Stable and unstable cosmological models in bimetric massive gravity. *Phys.Rev.*, D90:124014, 2014.
- [27] Edvard Mörtsell and Suhail Dhawan. Does the Hubble constant tension call for new physics? *JCAP*, 1809(09):025, 2018.
- [28] Manfred Lindner, Kevin Max, Moritz Platscher, and Jonas Rezacek. Probing alternative cosmologies through the inverse distance ladder. 2020.
- [29] Claudia de Rham, Lavinia Heisenberg, and Raquel H. Ribeiro. On couplings to matter in massive (bi-)gravity. *Class.Quant.Grav.*, 32(3):035022, 2015.
- [30] Yasuho Yamashita, Antonio De Felice, and Takahiro Tanaka. Appearance of Boulware-Deser ghost in bigravity with doubly coupled matter. *Int.J.Mod.Phys.*, D23:3003, 2014.
- [31] Marvin Lüben and Angnis Schmidt-May. Ghost-Free Completion of An Effective Matter Coupling in Bimetric Theory. *Fortsch. Phys.*, 66(6):1800031, 2018.
- [32] Claudia de Rham, Lavinia Heisenberg, and Raquel H. Ribeiro. Ghosts & Matter Couplings in Massive (bi-&multi-)Gravity. *Phys.Rev.*, D90:124042, 2014.
- [33] Yashar Akrami, Tomi S. Koivisto, and Adam R. Solomon. The nature of spacetime in bigravity: two metrics or none? *Gen.Rel.Grav.*, 47:1838, 2014.

- [34] Kurt Hinterbichler and Rachel A. Rosen. Note on ghost-free matter couplings in massive gravity and multigravity. *Phys. Rev.*, D92(2):024030, 2015.
- [35] Jonas Enander, Adam R. Solomon, Yashar Akrami, and Edvard Mortsell. Cosmic expansion histories in massive bigravity with symmetric matter coupling. *JCAP*, 01:006, 2015.
- [36] Adam R. Solomon, Jonas Enander, Yashar Akrami, Tomi S. Koivisto, Frank Könnig, et al. Cosmological viability of massive gravity with generalized matter coupling. *JCAP*, 1504:027, 2015.
- [37] A. Emir Gümrukçüoğlu, Lavinia Heisenberg, Shinji Mukohyama, and Norihiro Tanahashi. Cosmology in bimetric theory with an effective composite coupling to matter. *JCAP*, 1504(04):008, 2015.
- [38] A. Emir Gümrukçüoğlu, Lavinia Heisenberg, and Shinji Mukohyama. Cosmological perturbations in massive gravity with doubly coupled matter. *JCAP*, 1502:022, 2015.
- [39] Katsuki Aoki and Kei-ichi Maeda. Cosmology in ghost-free bigravity theory with twin matter fluids: The origin of dark matter. *Phys. Rev.*, D89(6):064051, 2014.
- [40] S.F. Hassan, Rachel A. Rosen, and Anngis Schmidt-May. Ghost-free Massive Gravity with a General Reference Metric. *JHEP*, 1202:026, 2012.
- [41] S.F. Hassan, Anngis Schmidt-May, and Mikael von Strauss. On Consistent Theories of Massive Spin-2 Fields Coupled to Gravity. *JHEP*, 1305:086, 2013.
- [42] Yashar Akrami, S. F. Hassan, Frank Könnig, Anngis Schmidt-May, and Adam R. Solomon. Bimetric gravity is cosmologically viable. *Phys. Lett.*, B748:37–44, 2015.
- [43] Atsushi Higuchi. Forbidden Mass Range for Spin-2 Field Theory in De Sitter Space-time. *Nucl.Phys.*, B282:397, 1987.
- [44] A. Higuchi. Massive Symmetric Tensor Field in Space-times With a Positive Cosmological Constant. *Nucl.Phys.*, B325:745–765, 1989.
- [45] D. Comelli, M. Crisostomi, and L. Pilo. Perturbations in Massive Gravity Cosmology. *JHEP*, 1206:085, 2012.
- [46] Giulia Cusin, Ruth Durrer, Pietro Guarato, and Mariele Motta. A general mass term for bigravity. *JCAP*, 1604(04):051, 2016.
- [47] Matteo Fasiello and Andrew J. Tolley. Cosmological Stability Bound in Massive Gravity and Bigravity. *JCAP*, 1312:002, 2013.
- [48] Frank Könnig. Higuchi Ghosts and Gradient Instabilities in Bimetric Gravity. *Phys.Rev.*, D91:104019, 2015.
- [49] Claudia de Rham, Lavinia Heisenberg, and Raquel H. Ribeiro. Quantum Corrections in Massive Gravity. *Phys.Rev.*, D88:084058, 2013.
- [50] Lavinia Heisenberg. Quantum corrections in massive bigravity and new effective composite metrics. *Class.Quant.Grav.*, 32(10):105011, 2015.
- [51] D. Comelli, M. Crisostomi, F. Nesti, and L. Pilo. Spherically Symmetric Solutions in Ghost-Free Massive Gravity. *Phys.Rev.*, D85:024044, 2012.
- [52] Valentina Baccetti, Prado Martin-Moruno, and Matt Visser. Massive gravity from bimetric gravity. *Class.Quant.Grav.*, 30:015004, 2013.
- [53] Claudia de Rham, J. Tate Deskins, Andrew J. Tolley, and Shuang-Yong Zhou. Graviton Mass Bounds. *Rev. Mod. Phys.*, 89(2):025004, 2017.
- [54] Adam G. Riess et al. Observational evidence from supernovae for an accelerating universe and a cosmological constant. *Astron.J.*, 116:1009–1038, 1998.
- [55] S. Perlmutter et al. Cosmology from Type Ia supernovae. *Bull. Am. Astron. Soc.*, 29:1351, 1997.
- [56] N. Suzuki, D. Rubin, C. Lidman, G. Aldering, R. Amanullah, et al. The Hubble Space Telescope Cluster Supernova Survey: V. Improving the Dark Energy Constraints Above $z > 1$ and Building an Early-Type-Hosted Supernova Sample. *Astrophys.J.*, 746:85, 2012.
- [57] Rev.Thomas Bayes. An essay toward solving a problem in the doctrine of chances. *Phil. Trans. Roy. Soc. Lond.*, 53:370–418, 1764.

- [58] Giulio D’Agostini. Probability and measurement uncertainty in physics: A Bayesian primer. 1995.
- [59] Roberto Trotta. Applications of Bayesian model selection to cosmological parameters. *Mon. Not. Roy. Astron. Soc.*, 378:72–82, 2007.
- [60] Roberto Trotta. Bayes in the sky: Bayesian inference and model selection in cosmology. *Contemp. Phys.*, 49:71–104, 2008.
- [61] Andrew R. Liddle. Statistical methods for cosmological parameter selection and estimation. *Ann. Rev. Nucl. Part. Sci.*, 59:95–114, 2009.
- [62] Nelson Christensen and Renate Meyer. Bayesian methods for cosmological parameter estimation from cosmic microwave background measurements. 2000.
- [63] Nelson Christensen, Renate Meyer, Lloyd Knox, and Ben Luey. II. Bayesian methods for cosmological parameter estimation from cosmic microwave background measurements. *Class. Quant. Grav.*, 18:2677, 2001.
- [64] Andrew Gelman and Donald B. Rubin. Inference from Iterative Simulation Using Multiple Sequences. *Statist. Sci.*, 7:457–472, 1992.
- [65] Antony Lewis and Sarah Bridle. Cosmological parameters from CMB and other data: A Monte Carlo approach. *Phys. Rev.*, D66:103511, 2002.
- [66] Dani Gamerman and Hedibert F. Lopes. *Markov Chain Monte Carlo: Stochastic Simulation for Bayesian Inference*. Chapman and Hall/CRC Texts in Statistical Science, 2006.
- [67] G. D’Amico, C. de Rham, S. Dubovsky, G. Gabadadze, D. Pirtskhalava, and A. J. Tolley. Massive Cosmologies. *Phys. Rev.*, D84:124046, 2011.
- [68] A. Emir Gümrukçüoğlu, Chunshan Lin, and Shinji Mukohyama. Open FRW universes and self-acceleration from nonlinear massive gravity. *JCAP*, 1111:030, 2011.
- [69] A. Emir Gümrukçüoğlu, Chunshan Lin, and Shinji Mukohyama. Cosmological perturbations of self-accelerating universe in nonlinear massive gravity. *JCAP*, 1203:006, 2012.
- [70] Babak Vakili and Nima Khosravi. Classical and quantum massive cosmology for the open FRW universe. *Phys.Rev.*, D85:083529, 2012.
- [71] Antonio De Felice, A. Emir Gümrukçüoğlu, and Shinji Mukohyama. Massive gravity: nonlinear instability of the homogeneous and isotropic universe. *Phys.Rev.Lett.*, 109:171101, 2012.
- [72] Matteo Fasiello and Andrew J. Tolley. Cosmological perturbations in Massive Gravity and the Higuchi bound. *JCAP*, 1211:035, 2012.
- [73] Antonio De Felice, A. Emir Gümrukçüoğlu, Chunshan Lin, and Shinji Mukohyama. Nonlinear stability of cosmological solutions in massive gravity. *JCAP*, 1305:035, 2013.
- [74] Rene Andrae, Tim Schulze-Hartung, and Peter Melchior. Dos and don’ts of reduced chi-squared. 12 2010.
- [75] Adam G. Riess et al. A 2.4% Determination of the Local Value of the Hubble Constant. *Astrophys. J.*, 826(1):56, 2016.
- [76] Marvin Lüben, Angnis Schmidt-May, and Juri Smirnov. Vainshtein Screening in Bimetric Cosmology. 2019.
- [77] N. Aghanim et al. Planck 2018 results. VI. Cosmological parameters. *Astron. Astrophys.*, 641:A6, 2020.
- [78] Katsuki Aoki, Kei-ichi Maeda, and Ryo Namba. Stability of the Early Universe in Bigravity Theory. *Phys. Rev.*, D92(4):044054, 2015.
- [79] Jonas Enander and Edvard Mortsell. On stars, galaxies and black holes in massive bigravity. *JCAP*, 1511(11):023, 2015.
- [80] Jonas Enander and Edvard Mörtsell. Strong lensing constraints on bimetric massive gravity. *JHEP*, 1310:031, 2013.
- [81] Stefan Sjors and Edvard Mortsell. Spherically Symmetric Solutions in Massive Gravity and Constraints from Galaxies. *JHEP*, 02:080, 2013.

- [82] J. H. Gundlach. Laboratory tests of gravity. *New J. Phys.*, 7:205, 2005.
- [83] Serge Reynaud and Marc-Thierry Jaekel. Tests of general relativity in the solar system. *Proc. Int. Sch. Phys. Fermi*, 168:203–217, 2009.
- [84] C. D. Hoyle, D. J. Kapner, Blayne R. Heckel, E. G. Adelberger, J. H. Gundlach, U. Schmidt, and H. E. Swanson. Sub-millimeter tests of the gravitational inverse-square law. *Phys. Rev.*, D70:042004, 2004.
- [85] E. G. Adelberger, Blayne R. Heckel, and A. E. Nelson. Tests of the gravitational inverse square law. *Ann. Rev. Nucl. Part. Sci.*, 53:77–121, 2003.
- [86] Frank Könnig and Luca Amendola. Instability in a minimal bimetric gravity model. *Phys.Rev.*, D90:044030, 2014.
- [87] Macarena Lagos and Pedro G. Ferreira. Cosmological perturbations in massive bigravity. *JCAP*, 1412(12):026, 2014.
- [88] E. Mortsell and J. Enander. Scalar instabilities in bimetric gravity: The Vainshtein mechanism and structure formation. *JCAP*, 1510(10):044, 2015.
- [89] Marcus Höggås, Francesco Torsello, and Edvard Mörtzell. On the stability of bimetric structure formation. *JCAP*, 04:046, 2020.